Check for updates

Recent advances in graphene-based materials for dye-sensitized solar cell fabrication

Edigar Muchuweni, [ID] † Bice S. Martincigh [ID] and Vincent O. Nyamori [ID] *

In the past few years, dye-sensitized solar cells (DSSCs) have received considerable research attention, as potential alternatives to the commonly used, but expensive, silicon-based solar cells owing to the low-cost, facile fabrication procedures, less impact on the environment, capability of working even under low incoming light levels, and flexibility of DSSCs. However, the relatively low power conversion efficiencies (PCEs) and poor long-term operational stability of DSSCs still limit their large-scale and commercial applications. As a consequence, this has prompted tremendous research effort towards the realization of high performance and sustainable devices, through tailoring of the properties of the various DSSC components, *via* approaches such as introducing novel materials and new synthesis techniques. Among these, the application of novel materials, especially carbon-based materials, such as graphene and its derivatives, is more appealing due to their excellent optoelectronic, mechanical, thermal and chemical properties, which give them ample potential to replace or modify the traditional materials that are commonly used in the fabrication of the various DSSC components. In addition, the low-cost, abundance, non-toxicity, large specific surface area, flexibility and superior stability of graphene-based materials have enabled their recent use as photoanodes, *i.e.*, transparent conducting electrodes, semiconducting layers and dye-sensitizers, electrolytes and counter electrodes in DSSCs. Recently, the introduction of graphene-based materials into DSSCs resulted in a pronounced increase in PCE from ~0.13 to above 12.00%. Thus, employing the recent breakthroughs can further improve the optoelectronic properties of the various DSSC components and, hence, close the gap between DSSCs and their silicon-based counterparts that are currently exhibiting desirable PCEs of above 26%. Therefore, this review focuses on the recent applications of graphene-based materials as photoanodes, electrolytes and counter electrodes, for the possible fabrication of all-carbon-based DSSCs. The limitations, merits and future prospects of graphene-based DSSCs are discussed, so as to improve their photovoltaic performance, sustainability and cost-effectiveness.

School of Chemistry and Physics, University of KwaZulu-Natal, Westville Campus, Private Bag X54001, Durban 4000, South Africa. E-mail: nyamori@ukzn.ac.za

† On leave from Bindura University of Science Education, Department of Engineering and Physics, Private Bag 1020, Bindura, Zimbabwe.

Edigar Muchuweni is a Post-doctoral Scholar in the School of Chemistry and Physics at the University of KwaZulu-Natal (UKZN) in Durban, South Africa. He has also served as Coordinator of the Postgraduate Seminar Series at Botswana International University of Science and Technology (BIUST) over the period 2016–2017. His research interests include: Solar Energy Materials, Nanotechnology and Materials Science. In the latter, his research group works on novel nanomaterials, such as carbon nanotubes, graphene, graphene oxide and reduced graphene oxide, for several applications including energy harvesting, conversion and storage devices.

Bice S. Martincigh is a Professor in Physical Chemistry in the School of Chemistry and Physics at the University of KwaZulu-Natal (UKZN) in Durban, South Africa. She is the leader of the Nanomaterials Pillar of the UKZN Nanotechnology Platform and has served as President of the South African Chemical Institute (SACI) over the period 2015–2017. Her research interests include: Photochemistry, Environmental Chemistry and Nanotechnology and Materials Science as applied to environmental remediation. Her research group have prepared nanomaterials for application in sunscreens, photocatalysis and wastewater remediation.

1. Introduction

Renewable energy sources, such as wind, geothermal, biomass and solar energy, have gained tremendous research interest in recent years, to address up-coming global issues, particularly the depletion of conventional energy resources, *e.g.*, fossil fuels, due to the ever-increasing energy demand, coupled with greenhouse gas emissions that lead to global warming and climate change.[1–4] Among the renewable energy sources, solar energy is more appealing owing to its natural abundance and environmentally friendly benefit, since it entails the provision of clean energy harvested from the Sun.[5]

In this regard, recent work has been focussing on the fabrication of third generation photovoltaic devices, such as organic solar cells (OSCs),[6,7] dye-sensitized solar cells (DSSCs),[8,9] and perovskite solar cells,[10,11] in an attempt to overcome the drawbacks of the first and second generation solar cells. Among the third generation devices, the efficient conversion of solar energy into electricity can be achieved by using DSSCs due to their high performance even under diffuse solar irradiance, ease of fabrication, low manufacturing cost, flexibility and incorporation of environmentally friendly materials.[12,13] However, the power conversion efficiency (PCE) and long-term operational stability of DSSCs are still unfavourable for practical applications, in comparison with silicon-based solar cells that have already been commercialized.[14] Therefore, more research is still being done, *e.g.*, to enhance photon harvesting, charge carrier generation and mobility, while suppressing carrier recombination, and minimizing electrolyte evaporation and leakages, through modifying or replacing the traditional materials that are commonly used to fabricate the various DSSC components, such as the photoanode, electrolyte and counter electrode. This if done, is envisaged to improve device performance and sustainability, which subsequently opens up avenues for the large-scale fabrication and commercialization of DSSCs.

Vincent O. Nyamori is a Professor and Academic Leader in the School of Chemistry and Physics at the University of KwaZulu-Natal (UKZN) in Durban, South Africa. He is also the coordinator of the UKZN Nanotechnology Platform and currently serves as the Immdiate Past President of the South African Chemical Institute (SACI). His research interests include: Green and Sustainable Chemistry, Organometallic Synthesis, and Nanotechnology and Materials Science. His research group has interests on advanced nanomaterials for various applications including catalysis and energy devices. These nanomaterials include carbon nanotubes, graphene, graphitic carbon nitride and organo–inorganic hybrid materials.

As a consequence, the low-cost, abundance, non-toxicity, high optical transparency, and competitive electrical conductivity of carbon-based materials, such as carbon nanorods, carbon nanotubes (CNTs), carbon nanofibers, carbon nanoribbons and graphene,[15–19] have made them to be widely studied as potential replacements or additives to the traditional materials that are being used in the fabrication of the various DSSC components.[20,21] Among these, graphene, a novel two-dimensional single layer of graphite with a hexagonal lattice structure, has merits in terms of its large specific surface area, wide absorption spectral range, lightweight, flexibility, and high mechanical, thermal and chemical stability,[22,23] which are all vital for DSSC fabrication.

Several synthesis techniques, including bottom-up approaches, such as chemical vapour deposition (CVD) and epitaxial growth, which involve the high-temperature synthesis of graphene using carbon molecules as building blocks, and top-down approaches, such as oxidation–reduction and mechanical exfoliation, which involve the separation of stacked layers of graphite,[24–26] have been employed to prepare graphene sheets. Among these, bottom-up approaches have drawbacks of low yield, difficulty to scale-up, complex substrate transfer and high cost. Hence, top-down approaches are gaining considerable research attention due to their simple fabrication procedures, easy scalability, good reproducibility, and low cost.[24–26]

Nonetheless, the chemical inertness of pristine graphene,[27] renders it insoluble in organic solvents; hence, pure graphene is incompatible with solution synthesis. As a result, the derivatives of graphene, such as graphene oxide (GO), which is an oxygen functionalized graphene sheet, and reduced graphene oxide (rGO), have been widely explored owing to their high solubility in organic solvents, which makes them compatible with the low-cost, facile, and large-scale solution synthesis.[28] Although GO exhibits an insulating character, the chemical or thermal reduction of GO to remove the oxygen functional groups helps restore electron delocalization, enhancing carrier transport, and thereby converting the electrically insulating GO into conducting graphene sheets.[29–31] Among the graphene synthesis routes, the reduction of GO and CVD, are the most commonly used approaches due to their capability for large-scale synthesis.

To the best of our knowledge, although the PCE of DSSCs is still low for practical applications, modifying the various DSSC components with novel materials, such as graphene-based materials, has proven to be an attractive option. Over the last three years (2018–2020), graphene-based DSSCs have exhibited a rapid increase in PCE from ~0.13%[32] to above 12.00%.[33] Thus, employing the recent breakthroughs is envisaged to significantly improve the optoelectronic properties of the DSSC components to make DSSCs compete with the already commercialized silicon-based solar cells currently displaying record-high PCEs of above 26%.[34] Nonetheless, relatively few studies have explored the latest research progress on applying graphene-based materials in the fabrication of DSSC components, which, if done, is expected to enable the fabrication of low-cost and more stable all-carbon-based devices. Also, many studies have concentrated on optimizing the PCE only, without

focussing on the long-term operational stability of DSSCs, which is indispensable for commercial applications. Hence, this review presents the current advances in graphene-based materials, as photoanodes, electrolytes and counter electrodes of DSSCs, coupled with the merits, limitations and new perspectives for the future realization of low-cost, high performance and sustainable devices for possible commercialization.

2. Basic working principle of a DSSC

A typical DSSC is made up of a photoanode, *i.e.*, a dye-coated semiconducting oxide layer on a transparent conducting electrode, an electrolyte containing a redox couple (commonly, iodide/triiodide (I^-/I_3^-)), and a catalyst-coated counter electrode (cathode), as shown in Fig. 1.

From Fig. 1, when light shines on a DSSC, the dye-molecule, initially in its ground state (S), absorbs an incident photon of energy, hv, and it becomes excited to a higher energy state (S*), as illustrated in eqn (1):[35–37]

$$S + hv \rightarrow S^* \quad (1)$$

The excited dye molecule is oxidized without any time delay, as illustrated in eqn (2), where S^+ is the oxidized dye molecule. Hence, an electron is injected into the conduction band of the semiconducting oxide film, where it freely flows to the external circuit *via* a transparent conducting electrode:[35–37]

$$S^* \rightarrow S^+ + e^- \quad (2)$$

On the other hand, the oxidized dye molecule is regenerated back to its ground state by electron donation from the I^- in the redox couple, as illustrated in eqn (3):[35–37]

$$S^+ + \tfrac{3}{2}I^- \rightarrow S + \tfrac{1}{2}I_3^- \quad (3)$$

Eventually, the circuit is completed through I^- regeneration, *via* the reduction of I_3^- at the counter electrode, by electron donation from the external circuit, as illustrated in eqn (4):[35–37]

$$\tfrac{1}{2}I_3^- + e^- \rightarrow \tfrac{3}{2}I^- \quad (4)$$

As a result, the continuous conversion of solar into electrical energy is achieved by repeating these processes, without any chemical transformation.[35–37] Therefore, in a DSSC, charge generation occurs at the semiconductor–dye interface, and charge transport proceeds through the semiconducting oxide layer and electrolyte, to and from the external circuit, *via* the transparent conducting electrodes and counter electrodes, respectively.

3. Characterization of DSSCs' performance

The photovoltaic performance of a DSSC is mainly characterized by measuring the current density–voltage (J–V) characteristics, shown in Fig. 2, under a solar simulator operating at air-mass 1.5 global (AM 1.5G) illumination with an incident power intensity of 100 mW cm^{-2}. This allows the determination of the PCE, which is largely dependent on the number of photons absorbed by the dye and charge carriers collected at the electrodes. Therefore, the PCE is given by the ratio of the power output (P_{out}) to the power input (P_{in}), *i.e.*, it is measured by the quantity of incoming light that can be converted into electrical energy per unit time.[38,39] The PCE is determined by investigating the photovoltaic parameters, such as open-circuit voltage (V_{oc}), short-circuit current density (J_{sc}) and fill factor (FF) according to eqn (5):[38–40]

$$PCE = \frac{P_{out}}{P_{in}} = \frac{J_{sc}V_{oc}FF}{P_{in}} \quad (5)$$

where P_{in} is the incident solar power. V_{oc} is the maximum potential difference measured across a solar cell when no current flows.[39,41] J_{sc} is the maximum current that flows through the cell when the potential difference across it is zero, *i.e.*, when the electrodes are short-circuited.[36,41] Hence, the current through an external load is always less than J_{sc}. FF is a measure of the solar cell's quality as a power source, given by the ratio of the maximum power delivered by the cell to a load, *i.e.*, maximum
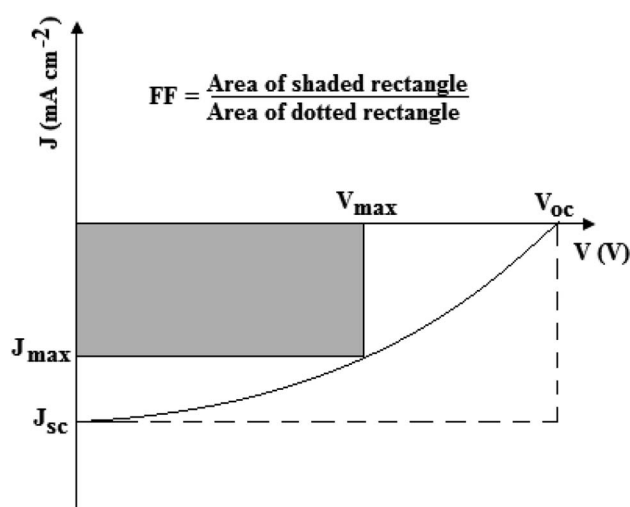

Fig. 1 A schematic diagram of the basic operation principle of a typical DSSC.

Fig. 2 A typical *J*–*V* curve for an illuminated DSSC.

power output of the cell to its theoretical power output, *i.e.*, its potential power output, and is determined by eqn (6):[38–40]

$$FF = \frac{J_{max} V_{max}}{J_{sc} V_{oc}} \qquad (6)$$

where V_{max} and J_{max} are the actual maximum voltage and current density, respectively, determined from the maximum power point on the J–V characteristics curve, as illustrated in Fig. 2. FF is used to determine the closeness of the cell's J–V characteristics to ideality, *i.e.*, it is a measure of the squareness of J–V curves. The optimal theoretical FF value is 1; however, in practice, it is less than 1, and values above 0.75 are deemed very good.[41,42]

4. Graphene-based photoanode

The photoanode usually consists of a layer of a dye-sensitized wide band gap nanocrystalline semiconductor metal oxide, on a transparent conducting electrode, as discussed in the following sub-sections.

4.1 Transparent conducting electrode

The conducting electrode is usually transparent, to allow the passage of light to the sensitizer, and is commonly made by depositing indium tin oxide (ITO) onto a glass substrate, due to the high optical transmittance in the visible range and high electrical conductivity of ITO. Nonetheless, ITO has shortcomings due to the scarcity, toxicity and high cost of indium (In), which is the main constituent element of ITO.[43–46] In addition, ITO is brittle and rigid, which limits its use on flexible substrates, and also good quality ITO requires expensive vacuum equipment and complex experimental procedures.

Although fluorine-doped tin oxide (FTO) has been used as a relatively low-cost alternative to ITO, the structural defects of FTO due to its rough surface often result in short circuits and leakage current,[47,48] which impair device performance, and hence limit its choice. Being motivated by the need to overcome these drawbacks, recent advanced materials, such as metal nanowires,[49,50] conductive polymers,[51,52] transparent conducting oxides,[53,54] CNTs,[55,56] and graphene,[57,58] have been proposed as potential replacements or additives to the conventional ITO and FTO electrodes. Among these, graphene-based materials are more appealing due to their high optical transmittance in the visible region, high electrical conductivity, excellent stability, easy availability, low-cost and non-toxicity.[58,59]

In this respect, Dong *et al.*[59] employed metal grids covered by graphene, as shown in Fig. 3, as transparent conducting electrodes in DSSCs. The graphene/platinum (Pt) and graphene/nickel (Ni) grid-based devices exhibited PCEs of 0.40 and 0.25%, respectively, in comparison with 0.17% for the reference devices with Pt grids only. This was attributed to the high electrical conductivity of graphene, which supplemented the collection of electrons from the semiconducting layer. In addition to their relatively higher PCEs, the graphene-based devices displayed excellent long-term stability and superior mechanical flexibility, which demonstrates the suitability of this novel

graphene-on metal grid transparent electrode, as a viable replacement for commonly used FTO and ITO electrodes.

This was improved by Song *et al.*[57] who deposited graphene-like carbon (GLC) thin films on FTO glass substrates, and used the composite films as transparent conducting electrodes in DSSCs. The addition of GLC thin films onto FTO led to a significant increase in the V_{oc}, J_{sc} and FF, which was attributed to the suppression of carrier recombination and improvement of the contacts at the semiconducting layer-transparent conducting electrode interface. As a result, the PCE increased from 5.90% for the bare FTO substrate, to 6.92% for the GLC/FTO-based devices.

Also, since the work function of graphene (-4.4 eV) is more negative than the conduction band of titanium dioxide (TiO$_2$) (-4.2 eV), the incorporation of graphene between TiO$_2$ and FTO, permits electron transport from TiO$_2$ to graphene, while blocking electron transport in the reverse direction.[60] In addition, the work function of graphene is almost similar to that of FTO, hence, the surface modification of FTO by graphene acts as an additional electron collecting electrode, which significantly enhances the charge transport rate in the transparent conducting electrode,[60] thereby, improving device performance. On the other hand, the porous TiO$_2$ layer often leaves some uncovered gaps on the bare FTO conducting surface, which allows the redox electrolyte solution to penetrate, reaching the bare FTO substrate, resulting in direct carrier recombination, and hence reduces the device performance.[61] Therefore, surface modification of the FTO substrate is vital for the fabrication of high performance DSSCs.

In this regard, Roh *et al.*[62] employed rGO-modified FTO substrates as transparent conducting electrodes in DSSCs. The rGO sheets had very few defects and were firmly attached to the FTO surface, which helped to minimize the charge transfer resistance and electron–hole recombination at the TiO$_2$–FTO interface, resulting in a high charge transfer rate, and subsequently high PCEs of 8.44%. Interestingly, the devices with rGO-modified transparent conducting electrodes outperformed those with bare FTO substrates, and those subjected to the conventional surface modification by hydrolyzing a titanium tetrachloride (TiCl$_4$) aqueous solution, demonstrating the potential of graphene-functionalized FTO substrates to improve device performance.

In another study, Selopal *et al.*[63] prepared few-layers of large-area continuous graphene films *via* the CVD technique, as illustrated in Fig. 4 (a), and used them as transparent conducting electrodes in DSSCs, which displayed a best PCE of 2%. This was associated with the homogeneous, continuous and highly crystalline nature of the prepared films, which facilitates ballistic charge transport through the whole graphene sheet, thereby, increasing the electrical conductivity, and hence improving the device performance.

Recently, Shahid *et al.*[61] modified the surface of FTO glass substrates with graphene nanoplatelets (GNPLs), which provided additional conducting bridges for the photo-injected electrons, and increased the J_{sc} as illustrated in Fig. 4 (b). As a result, the DSSCs with the GNPLs/FTO transparent conducting electrodes exhibited a PCE of 2.32%, which was higher than
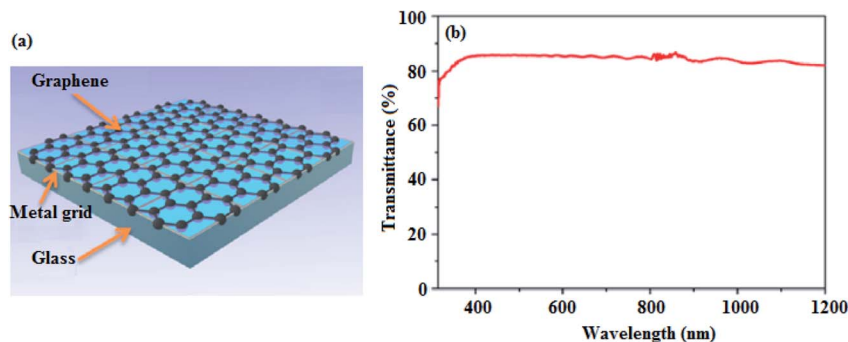
Fig. 3 (a) The hybrid graphene/metal grid transparent conducting electrode, and (b) the optical transmittance spectrum of the graphene/Ni electrode.[59]
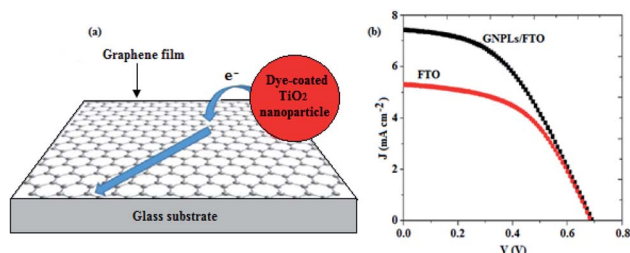

Fig. 4 (a) A schematic illustration of electron injection from a dye-coated TiO_2 nanoparticle and transport in a continuous graphene film,[63] and (b) the $J-V$ characteristics of DSSCs based on GNPLs/FTO and pristine FTO electrodes.[61]

1.86% for the pristine FTO-based DSSCs. This revealed the significance of using graphene-based materials to modify the conventional FTO substrate. Also, Al-Rawashdeh *et al.*[64] employed rGO/ZnO composite electrodes in DSSCs, which inhibited carrier recombination, and enhanced J_{sc}, resulting in devices with a PCE of 0.45%, which outperformed the devices without GO. Therefore, the preparation of graphene-based nanocomposite electrode materials, with complementary opto-electronic properties, could enable the use of graphene and its derivatives, as replacements for the commonly used metal oxide front electrodes.

The photovoltaic parameters of DSSCs employing graphene-based materials as transparent conducting electrodes (discussed in this review) are summarized in Table 1. Among these, devices with rGO/FTO composite transparent electrodes exhibited the best PCE of 8.44%,[62] which outperformed the devices based on conventional FTO and ITO transparent electrodes. Therefore, further work on optimizing the optoelectronic properties of hybrid rGO/FTO transparent conducting glass substrates is envisaged to yield favourable device performance, as a link bridge towards commercialization.

4.2 Semiconducting layer

In a DSSC, the mesoporous semiconducting layer plays a significant role in the photon to electricity conversion process.[65] Hence, the semiconducting layer should have a large surface area for maximum sensitizer loading, a high electrical conductivity for effective collection and transportation of electrons to the transparent electrode, and a porous membrane for efficient diffusion of the redox couple.[66,67] The semiconducting layer materials used in DSSCs include TiO_2, ZnO, SnO_2, Nb_2O_5 and Fe_3O_4.[68,69] Among these, nanocrystalline anatase TiO_2 is commonly used due to its low-cost, abundance, non-toxicity and high photochemical stability.[70,71] However, TiO_2 has shortcomings in terms of its relatively low optical transparency and inefficient light scattering ability, which result in poor light harvesting, and hence lowers the device performance.[72] Also, TiO_2 is negatively affected by its relatively low number of carriers in the conduction band, poor electron transport, and high charge carrier recombination,[73–76] which in turn reduce the PCE.

As a result, the incorporation of graphene-based materials into the semiconducting metal oxide layer has received significant research attention, due to the large specific surface area of graphene of $\sim 2.63 \times 10^3$ m^2 g^{-1},[77] high optical transmittance of 97.7% in the visible region,[78] and faster electron mobility of 15 000 cm^2 V^{-1} s^{-1}, when compared to 0.1–0.4 cm^2 V^{-1} s^{-1} for TiO_2 and 200–1000 cm^2 V^{-1} s^{-1} for ZnO.[79] Furthermore, the energy level of graphene lies between the conduction band of TiO_2 and FTO, which facilitates the efficient transportation of electrons from TiO_2 to FTO, and hence suppresses back charge transfer losses, thereby, enhancing the performance of graphene-based DSSCs.[69]

In this regard, Ramli *et al.*,[80] Chong *et al.*,[81] Manikandan *et al.*,[82] and Yau *et al.*,[83] incorporated GO into TiO_2, and employed the resulting nanocomposites as semiconducting

Table 1 Photovoltaic parameters of DSSCs employing graphene-based transparent conducting electrodes

Transparent electrode	V_{oc} (V)	J_{sc} (mA cm^{-2})	FF	PCE (%)	Ref.
Graphene/Pt grids	0.43	2.87	0.32	0.40	59
Graphene/Ni grids	0.33	1.33	0.57	0.25	59
GLC/FTO	0.71	15.60	0.63	6.92	57
rGO/FTO	0.68	18.95	0.65	8.44	62
Graphene	0.63	7.80	0.40	2.00	63
GNPLs/FTO	0.69	7.41	0.45	2.32	61
rGO/ZnO	0.39	2.59	0.45	0.45	64

layers in DSSCs. This enhanced dye loading owing to the large surface area and mesoporous structures of GO/TiO$_2$, which in turn improved photon harvesting and reduced the charge transfer resistance at the dye–TiO$_2$ and TiO$_2$–FTO interfaces. This resulted in GO/TiO$_2$-based devices with PCEs of 3.70, 6.86, 8.62 and 6.25%, respectively, which generally outperformed the DSSCs based on pristine TiO$_2$. Therefore, the integration of GO with TiO$_2$ improves the photocatalytic activity and electron injection rate from the excited dye to the conduction band of the GO/TiO$_2$ film, and eventually to the FTO substrate. This in turn, suppresses charge carrier recombination, which increases the electron lifetime, and hence improves the device performance.

In another study, Nien et al.[84] co-incorporated GO and silver (Ag) into TiO$_2$ nanofiber semiconducting layers, as shown in Fig. 5 (a), which provided a large surface area and more active sites for dye adsorption, and hence facilitated more light absorption for effective photoelectron generation, and created numerous pathways for electron transport to the FTO electrode. This suppressed charge carrier recombination, and resulted in devices with a relatively higher PCE of 5.33%, as compared to 4.46 and 3.79% for the TiO$_2$/GO and pristine TiO$_2$-based devices, respectively, demonstrating the significance of doping towards improving device performance.

Wang et al.[85] also employed GO and zinc aluminium mixed metal oxide (ZnAl-MMO) as a composite semiconducting layer in DSSCs that exhibited a PCE of 0.55%, which was higher than 0.41% for the ZnAl-MMO-based devices, without GO. The improvement in device performance was attributed to the larger specific surface area of GO, which increased the dye loading ability, and hence improved the photon harvesting and photocurrent generation, resulting in an enhanced J_{sc}, as shown in Fig. 5 (b), and hence improved device performance.

Unlike GO which is an insulator, rGO is conductive, thus, it can be used to provide more efficient charge transport pathways between the dye and TiO$_2$, which suppress electron–hole recombination, and hence improve device performance.[86] In this respect, rGO has been employed to modify the TiO$_2$ semiconducting layer, resulting in DSSCs with PCEs, such as 7.20,[87] 7.48,[88] 7.68,[89] 8.51,[90] 4.43[76] and 6.90%,[91] which generally outperformed their pristine TiO$_2$, rGO and GO/TiO$_2$ counterparts. In addition, rGO-based ternary nanocomposites, such as TiO$_2$/cadmium sulfide (CdS)/rGO,[92] rGO/graphene/TiO$_2$,[18] and Ag/rGO/TiO$_2$,[93,94] have also been used as semiconducting layers in

DSSCs, which helped to increase the electron transfer rate and mobility. This resulted in devices with PCEs of 6.50, 11.80, 6.87 and 9.15%, respectively, which outperformed the corresponding TiO$_2$ reference device, thereby, revealing the importance of employing graphene-based nanocomposites in future research to enhance device performance. Recently, Le et al.[95] replaced TiO$_2$ with a ZnO/rGO composite semiconducting layer in DSSCs, which displayed a PCE of 1.55%. Although the PCE was low, this outperformed the ZnO reference device, which had a PCE of 1.08%, thereby, demonstrating the significance of using graphene-based composites in improving device performance.

Graphene/TiO$_2$ composite films have also been employed as semiconducting layers in DSSCs, which enhanced dye loading for effective light harvesting, and provided efficient electron transport pathways, which increased the electron lifetime and reduced carrier recombination. This resulted in DSSCs with optimum PCEs of 1.32[96] and 1.47%,[97] which outperformed 1.18 and 0.66%, respectively, for the devices based on pure TiO$_2$, demonstrating the significance of graphene/TiO$_2$ nanocomposites in improving device performance.

Although, SnO$_2$ has been used as a potential alternative to the conventional TiO$_2$ semiconducting layer, it has shortcomings of poor dye adsorption and slow electron transfer rate, both of which impair device performance.[98] Interestingly, these drawbacks can be addressed by using a hybrid semiconducting layer, such as TiO$_2$/SnO$_2$/graphene, proposed by Basu et al.,[99] which increases dye loading and electron transfer rate, as illustrated in Fig. 6, and hence in their case, resulted in a ~16% increment in PCE to 3.37%, i.e., from 2.91% for the TiO$_2$/SnO$_2$ control device, assembled without graphene. In addition, the TiO$_2$/SnO$_2$/graphene-based devices displayed superior stability, as revealed by their ability to retain 92% of their initial PCE after 200 h of illumination, as compared to the TiO$_2$/SnO$_2$ control devices, which retained 70% of the original PCE under the same conditions.

In addition, the synergistic effect between N–TiO$_2$ and graphene,[100] MoS$_2$ and graphene,[101] and NiS$_2$ and graphene,[33] facilitates the formation of composite semiconducting layers with large surface areas, porous structures and continuous interpenetrating networks for efficient photon harvesting, photocurrent generation and electron transport, resulting in DSSCs with PCEs of 5.01, 8.92 and 12.56%, respectively. TiO$_2$/GQDs have also been used as semiconductor layers, which increased dye adsorption and reduced charge carrier recombination, resulting in DSSCs with PCEs of 4.40[102] and 5.01%.[103]

The photovoltaic parameters of DSSCs with graphene-based semiconducting layers (discussed in this review) are
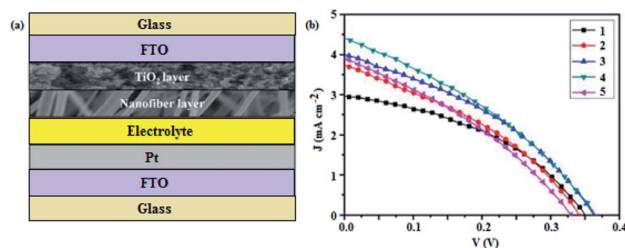

Fig. 5 (a) A schematic diagram of the GO/TiO$_2$/Ag-based DSSC,[84] and (b) the J–V characteristics of DSSCs based on: (1) ZnAl-MMO 8 : 1, (2) ZnAl–10 ml GO, (3) ZnAl–20 ml GO, (4) ZnAl–30 ml GO, and (5) ZnAl–40 ml GO, semiconducting layers.[85]
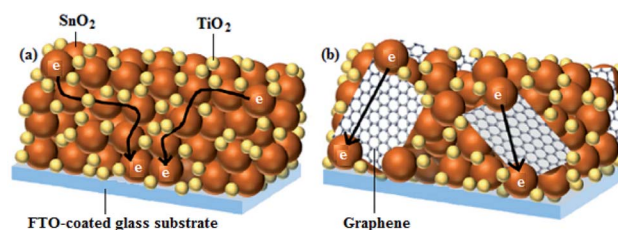

Fig. 6 An illustration of electron transport (a) in the TiO$_2$/SnO$_2$, and (b) TiO$_2$/SnO$_2$/graphene photoanodes.[99]

summarized in Table 2. Among these, devices with a graphene/NiS_2 composite semiconducting layer exhibited the best PCE of 12.56%.[33] This suggests that with the future development of novel graphene-based composites consisting of large surface areas and excellent distribution of pores for more dye loading, enhanced photon harvesting, effective carrier generation, and efficient carrier transport can be achieved, resulting in superior device performance.

4.3 Photosensitizer

The dye or photosensitizer plays a prominent role in harvesting the incoming light, and injecting the photoexcited electrons into the conduction band of the semiconducting material, *i.e.*, it is responsible for absorbing the incident solar energy, and converting it into electrical energy.[104,105] Therefore, an effective photosensitizer should have a broad and intense absorption spectrum that covers the entire visible region, high adsorption affinity to the surface of the semiconducting layer, excellent stability in its oxidized form, low-cost and low threat to the environment.[105] Furthermore, its lowest unoccupied molecular orbital (LUMO) level, *i.e.*, excited state level, must be higher in energy than the conduction band edge of the semiconductor, for efficient electron injection into the conduction band of the semiconductor.[106,107] Also, its highest occupied molecular orbital (HOMO) level, *i.e.*, oxidized state level, must be lower in energy than the redox potential of the electrolyte, to promote dye regeneration.[106,107]

The most commonly used photosensitizers are ruthenium-based complexes owing to their wide absorption range, *i.e.*,

Table 2 Photovoltaic parameters of DSSCs employing graphene-based semiconducting layers

Semiconducting layer	V_{oc} (V)	J_{sc} (mA cm^{-2})	FF	PCE (%)	Ref.
GO/TiO$_2$	0.72	9.80	0.53	3.70	80
GO/TiO$_2$	0.73	16.21	0.58	6.86	81
GO/TiO$_2$	0.79	20.60	0.53	8.62	82
GO/TiO$_2$	0.66	14.78	0.64	6.25	83
GO/TiO$_2$	0.71	8.98	0.70	4.46	84
GO/TiO$_2$/Ag	0.78	9.79	0.70	5.33	84
GO/ZnAl-MMO	0.37	4.46	0.34	0.55	85
rGO/TiO$_2$	0.54	28.36	0.47	7.20	87
rGO/TiO$_2$	0.74	15.29	0.66	7.48	88
rGO/TiO$_2$	0.78	14.68	0.67	7.68	89
rGO/TiO$_2$	0.63	25.02	0.54	8.51	90
rGO/TiO$_2$	0.65	10.92	0.62	4.43	76
rGO/TiO$_2$	0.59	16.27	0.72	6.90	91
TiO$_2$/CdS/rGO	0.66	13.27	0.75	6.50	92
rGO/graphene/TiO$_2$	0.71	26.00	0.64	11.80	18
Ag/rGO/TiO$_2$	0.73	14.08	0.66	6.87	93
Ag/rGO/TiO$_2$	0.78	14.30	0.82	9.15	94
ZnO/rGO	0.64	3.02	0.60	1.55	95
Graphene/TiO$_2$	0.76	2.26	0.65	1.32	96
Graphene/TiO$_2$	0.66	5.15	0.44	1.47	97
TiO$_2$/SnO$_2$/graphene	0.65	9.03	0.58	3.37	99
N–TiO$_2$/graphene	0.71	15.38	0.46	5.01	100
Graphene/MoS$_2$	0.82	15.82	0.71	8.92	101
Graphene/NiS$_2$	0.89	23.13	0.85	12.56	33
TiO$_2$/GQDs	0.73	11.54	0.53	4.40	102
TiO$_2$/GQDs	0.69	14.22	0.51	5.01	103

from the visible to the near-infrared (NIR) region, which renders them with superior photon harvesting properties,[108] and excellent metal-to-ligand charge transfer.[109] However, these complexes require multi-step synthesis reactions, and they contain a heavy metal, which is expensive, scarce and toxic.[110] As a result, metal-free dyes, such as natural dyes, *e.g.*, from fruits, flowers, leaves and algae, coupled with their organic derivatives have attracted considerable research interest, owing to their low-cost, simple synthesis procedure, abundance in nature, non-toxicity, and high molar absorption coefficient.[35,111,112] Nonetheless, on their own, natural dyes, are the least efficient, and often result in DSSCs with very low performance due to their relatively narrow and less intense absorption spectrum in the visible region, and poor carrier dissociation and injection capability at the TiO$_2$-dye interface.[113]

In this regard, the wide and intense absorption spectrum of graphene, which enables each single layer to absorb 2.3% of the incoming light,[78] renders graphene-based materials with a promising potential as alternative photosensitizers for the fabrication of less expensive and greener DSSCs. Furthermore, the work function of graphene, which lies between the conduction bands of FTO (or ITO) and TiO$_2$, promotes the effective transfer of the photogenerated electrons from TiO$_2$ to FTO (or ITO), with minimum recombination, thereby, improving device performance.[114]

As a consequence, Ismail *et al.*[115] incorporated GO into the mangosteen natural dye, which led to a decrease in the charge transfer resistance in the TiO$_2$ layer, thereby, inhibiting carrier recombination, and increasing the electron lifetime, due to the additional electron conduction pathways provided by graphene. This improved the PCE from 0.31% for the DSSCs with the mangosteen dye only, to 0.40% for the GO/mangosteen-based devices. Therefore, with the current drive towards low-cost and environmentally friendly devices, the use of natural dyes modified by graphene-based materials, as sensitizers, could become an attractive avenue for future research.

Metal organic frameworks (MOFs) have also been proposed as potential photosensitizer materials owing to their low-cost, excellent stability, ease of processing, hierarchically ordered structure, biocompatibility, and superior light harvesting properties.[116–118] Hence, their synergy with graphene to form a hybrid photosensitizer material could result in favourable properties, as demonstrated by Kaur *et al.*[116] who employed graphene/MOF composite photosensitizers in DSSCs. The graphene/MOF-based devices displayed a higher PCE of 2.2%, when compared to 0.27 and 0.46%, for MOF[117] and MOF/CNT-based devices,[118] respectively. This was attributed to the low charge transfer resistance due to the efficient collection of electrons by the resulting graphene/MOF/TiO$_2$/FTO photoanode, demonstrating the potential of graphene/MOF composite photosensitizers for the future development of novel photoanodes in DSSCs.

In another study, Gatti *et al.*[119] fabricated greener DSSCs by using rGO and a metal-free donor–π–acceptor (D–π–A) dye, *i.e.*, triphenylamino (D)–thiophene (π)–cyanoacrylic acid (A) (TPA–Th–H) dye, as a composite sensitizer. Although this resulted in devices with a lower J_{sc}, as illustrated in Fig. 7, and a lower PCE

of 0.8% due to lower dye loading, in comparison with 3.5% for the cell with the TPA–Th–H reference dye, the rGO/TPA–Th–H composite sensitizer was strongly anchored to the surface of the semiconducting layer, demonstrating its enhanced chemical stability, vital for the future development of sustainable devices. Wahab et al.[120] also incorporated rGO into ruthenium-based dyes, and fabricated DSSCs with a PCE of 0.02%, which outperformed the ruthenium-based control devices that had a PCE of 0.005%, demonstrating the suitability of rGO as a promising dye-additive, capable of enhancing device performance.

Volland et al.[121] also prepared a hybrid photosensitizer consisting of a NIR-absorbing azulenocyanine, as an electron donor, and few-layer graphene, as an electron acceptor, which exhibited a wide absorption spectrum, from the ultraviolet (UV) to the NIR region, for effective light harvesting, and better electron transport properties for suppressing carrier recombination. As a result, the graphene/azulenocyanine/di-tetrabutylammonium cis-bis(isothiocyanato)bis(2,2′-bipyridyl-4,4′-dicarboxylato)ruthenium(II) (N719)-based DSSCs displayed a PCE of 8.32%, in comparison with 7.47 and 5.65% for the graphene/N719 and TiCl₄/N719-based devices.

On the other hand, the tunable optical band gap, high absorption coefficient and excellent band alignment of low band gap semiconductor quantum dots (QDs), such as CdS, cadmium selenide (CdSe), cadmium telluride (CdTe), lead(II) sulfide (PbS), and lead selenide (PbSe), enable them to be used as photosensitizers in DSSCs.[122–125] However, the Cd or Pb-based elements are highly toxic and, hence, hazardous to health.[32] Therefore, graphene QDs (GQDs) have been investigated as potential sensitizer alternatives due to their non-toxicity, tunable optical band gap, and wide absorption spectral range.[126]

In this regard, Zamiri and Bagheri,[127] replaced the N719 dye with GQDs, and observed an increase in PCE from 1.13 to 1.26%, which was attributed to the closeness of the conduction band of the GQDs to that of the ZnO semiconducting layer, in comparison with the conduction band of N719. Majumder and Mondal,[32] also fabricated DSSCs with PCEs of 0.13, 0.25 and 0.29% for the GQD, N-GQD, and sulfur-nitrogen co-doped GQD (SN-GQD) photosensitizers, respectively. This was improved by
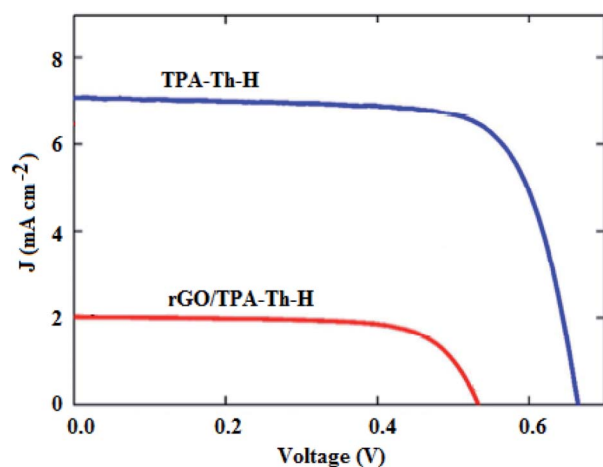
Jahantigh et al.[128] and Yang et al.,[129] who respectively incorporated N-GQDs and oxygen functionalized GQDs into the N719 dye, as illustrated in Fig. 8. This resulted in an increase in PCE from 5.72% for the devices based on pristine N719 dye, to 7.49% for the N-GQD/N719-based DSSCs,[128] and from 7.6% for the N719 dye devices, to 8.9% for the GQD/N719-based DSSCs.[129] Besides producing a significant increase in device performance, the GQDs reduced the quantity of the N719 dye used, which reduced the cost and environmental impact, thus, revealing the potential of GQDs as promising metal-free and 'green' alternatives to the ruthenium-based dyes in DSSCs.

Recently, being motivated by the increasing demand to replace the expensive, rare and toxic metal complexes, with low-cost and environmentally friendly photosensitizers, Saedi et al.[35] incorporated GQDs into natural dyes, extracted from green (Ulva) and red (Gracilaria) algae. The Gracilaria/GQD-based devices exhibited the best PCE of 0.94%, as compared to 0.39, 0.52, and 0.81%, for the DSSCs with Ulva, Gracilaria and Ulva/GQD photosensitizers, respectively. This was attributed to the wider absorption peak of the Gracilaria/GQD composite sensitizer, in the visible region, which facilitates the harvesting of more sunlight for efficient photoelectron generation.

The photovoltaic parameters of DSSCs employing graphene-based photosensitizers (discussed in this review) are summarized in Table 3. Among the devices based on natural dyes, the DSSCs with Gracilaria/GQD composite photosensitizers exhibited the best PCE of 0.94%,[35] and among the ruthenium-based devices, the DSSCs with graphene/azulenocyanine/N719 and GQDs/N719 composite photosensitizers exhibited the best PCEs of 8.32[121] and 8.90%,[129] respectively. This reveals the significance of using low-cost and environmentally friendly graphene-based composite photosensitizers to improve device performance, while at the same time reducing dependency on expensive, scarce and toxic ruthenium-based dyes.

5. Graphene-based electrolyte

The role of the electrolyte is to conduct holes through the redox couple (commonly, I^-/I_3^-), and to regenerate the oxidized dye molecules.[130,131] A good electrolyte should have high thermal

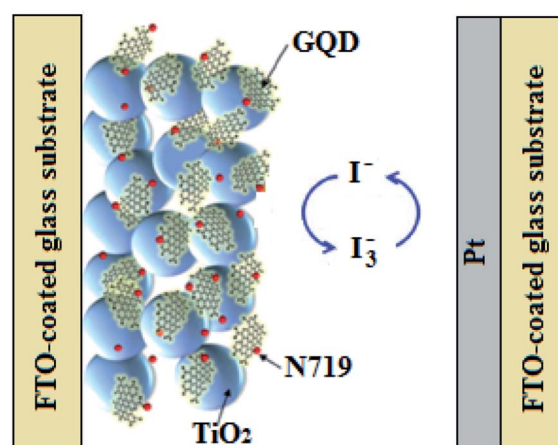Fig. 7 J–V curves for the rGO/TPA–Th–H and TPA–Th–H-based DSSCs.[119]

Fig. 8 A schematic diagram of the GQD/N719-based DSSC.[129]

and electrochemical stability, a high diffusion coefficient, low vapour pressure, appropriate viscosity, and ease of sealing, without suppressing charge carrier transport.[132,133]

The commonly used electrolytes in traditional DSSCs are liquid electrolytes, i.e., volatile organic solvents, due to their high diffusion coefficients and low viscosities.[134] However, these organic solvents have shortcomings in terms of high temperature instability, corrosion of electrodes over time, desorption of attached dye, toxicity, flammability, volatilization and leakage problems,[132,135–138] which limit their long-term performance, thereby, hindering the commercialization of DSSCs.

To overcome these drawbacks, novel solid or quasi-solid state electrolytes, such as hole transportation materials,[139,140] p-type semiconductors,[141,142] and polymer-based gel electrolytes,[143,144] have been developed as potential alternatives to the volatile liquid electrolytes. Among these, the polymer-based gel electrolytes are more appealing due to their negligible vapour pressure, non-flammability, and good contact with the semiconducting layer and counter electrode.[136,145] However, the polymers require conventional volatile organic solvents that act as plasticizers,[146,147] which subsequently give rise to flammability and high temperature instability.[148] In addition, the poor ionic conductivity of the polymer electrolytes, often results in DSSCs with lower PCEs than those of devices based on organic solvent electrolytes.[149] As a result, ionic liquid (IL)-based electrolytes have attracted considerable research attention due to their chemical and thermal stability, high ionic conductivity, tunable viscosity, non-volatility, and negligible vapour pressure.[150,151] Nonetheless, the PCEs of DSSCs based on IL electrolytes are still lower than those of devices based on organic solvent electrolytes,[134] and also the leakage problems of ILs, limit their long-term operational stability, which restricts their application.[152]

In this regard, carbon-based materials, such as graphene and its derivatives, have received considerable research attention as promising additives for enhancing the ionic conductivity and stability of polymer and IL electrolytes, due to the remarkable optical, electrical, mechanical, thermal and chemical properties of graphene.[134,149] Also, graphene/polymer or graphene/IL nanocomposites, result in the formation of interconnected networks, which not only provide efficient electron transport pathways through the electrolyte, but also enable the formation of quasi-solid state electrolytes, which reduce electrolyte evaporation and leakage, thereby, improving long-term operational stability.[153]

Being motivated by this, Lin et al.[154] employed poly(IL)/IL/GO composite gel electrolytes containing poly(1-butyl-3-vinylimidazolium bis(trifluoromethanesulfonyl) imide) ([PBVlm][TFSI]), PMII and GO. This resulted in more stable DSSCs with a best PCE of 4.83%, in comparison with 1.46% for devices without GO-based electrolytes, and was ascribed to the formation of a gel network, which prevented the leakage of the electrolyte's IL, demonstrating the potential of the quasi-solid state electrolytes in overcoming the drawbacks of volatile liquid electrolytes. In addition, Kowsari and Chirani,[155] also incorporated GO-hexa-methylene tri-butyl-ammonium iodide (GO-HMA-TBAI) and GO-hexa-methylene tri-methyl-ammonium iodide (GO-HMA-TMAI) into the PMII/1, 3-dimethylimidazolium iodide (DMII) composite IL electrolyte. This significantly improved the PCE from 3.96% of the IL-based reference device to 5.09, 6.78 and 8.33% for the GO, GO-HMA-TMAI/PMII-DMII and GO-HMA-TBAI/PMII-DMII-based DSSCs, respectively.

Khannam et al.[153] also prepared quasi-solid state electrolytes by incorporating GO into gelatin gel-based polymer electrolytes. This enhanced the ionic conductivity and stability of the electrolytes due to the formation of interconnected GO networks within the gelatin electrolyte matrix, resulting in highly stable DSSCs with a PCE of 4.02%, in comparison with 0.44% for the pristine gelatine electrolyte reference devices. In addition, Venkatesan et al.[156] used GO as a nanofiller for poly(vinylidene fluoride) (PVDF)/poly(ethylene oxide) (PEO)-based electrolytes, resulting in more stable DSSCs with a PCE of 8.78%, which was comparable to their pristine polymer-based counterparts. Hence, the synergy between graphene-based materials and volatile liquid or polymer electrolytes, promotes the fabrication of high performance and sustainable DSSCs, through the formation of quasi-solid state electrolytes, which eliminate the major shortcomings of pure liquid electrolytes, such as

Table 3 Photovoltaic parameters of DSSCs with graphene-based photosensitizers

Photosensitizer	V_{oc} (V)	J_{sc} (mA cm^{-2})	FF	PCE (%)	Ref.
GO/mangosteen	0.61	1.00	0.66	0.40	115
Graphene/MOF	0.45	20.00	0.44	2.2	116
rGO/TPA–Th–H	0.53	2.02	0.70	0.80	119
Graphene/azulenocyanine/N719	0.80	17.01	0.60	8.32	121
Graphene/N719	0.83	14.98	0.60	7.47	121
GQDs	0.64	3.17	0.62	1.26	127
GQDs	0.37	0.87	0.40	0.13	32
N-GQDs	0.37	1.51	0.43	0.25	32
SN-GQDs	0.36	1.84	0.45	0.29	32
N-GQDs	0.48	1.49	0.53	0.37	128
N-GQDs/N719	0.72	17.65	0.59	7.49	128
GQDs/N719	0.72	19.60	0.66	8.90	129
Gracilaria/GQDs	0.73	2.26	0.56	0.94	35
Ulva/GQDs	0.75	2.04	0.52	0.81	35

electrolyte leakage and evaporation, coupled with the low ionic conductivity of polymer electrolytes.

The incorporation of rGO into polymer electrolytes, such as PEO,[157] poly(methyl methaacrylate) (PMMA)[158] and PEO/PVDF-hexafluoro propylene (HFP),[159,160] as illustrated in Fig. 9, has also been reported to result in the fabrication of more stable DSSCs, with PCEs of 5.07, 5.38, 4.58 and 4.24%, respectively. Interestingly, the rGO-based DSSCs outperformed the pure polymer electrolyte-based control devices, which was associated with the increase in ionic conductivity, charge carrier concentration, diffusion coefficient and stability of the composite electrolytes. Recently Manafi et al.[161] incorporated polyethylene glycol (PEG)-modified GNPLs into the PEO/PVDF-HFP polymer gel electrolyte of DSSCs, which enhanced the ionic conductivity, resulting in a significant increase in PCE from 0.62% for the DSSCs based on PEO/PVDF-HFP polymer electrolytes to 5.45% for the GNPLs:PEG-PEO/PVDF-HFP devices.

Zheng[162] and Rehman et al.,[163] also incorporated graphene into poly(acrylic acid) (PAA)/PEG and polyvinyl acetate (PVAc) polymer gel electrolytes, respectively, and fabricated more stable DSSCs with PCEs of 9.10 and 4.57%. The graphene-based devices generally outperformed the pristine polymer and liquid electrolyte reference devices, which was attributed to an increase in catalytic activity and shorter charge transfer length, and hence excellent charge kinetics, due to the presence of more stable and conducting graphene channels within the composite liquid and polymer gel electrolytes.

Recently, Porfarzollah et al.[152] integrated GQDs with an imidazolium-based IL, which enhanced the long-term stability of the electrolyte, and inhibited back electron transfer to the electrolyte, thereby suppressing carrier recombination, and increasing the electron lifetime. As a result, the hybrid quasi-solid state electrolyte-based DSSCs exhibited a PCE of 4.57%, in comparison with 2.23 and 4.52%, for the GQDs and IL-based devices, respectively. Therefore, with further optimization of parameters, the GQDs-IL composite electrolyte is expected to overcome the leakage problems of IL and liquid electrolytes.

The photovoltaic parameters of DSSCs employing graphene-based electrolytes (discussed in this review) are summarized in Table 4. Among these, devices with PEO/PVDF-GO and graphene-PAA/PEG quasi-solid state electrolytes exhibited the best PCEs of 8.78 [156] and 9.10%,[162] respectively. Furthermore, the graphene-based quasi-solid state electrolytes helped to overcome the evaporation and leakage problems associated with organic solvent and IL electrolytes, and also increased the ionic conductivity of the polymer electrolytes.

6. Graphene-based counter electrode

The counter electrode collects electrons from the external circuit and injects them into the electrolyte to catalyze the reduction of I_3^- to I^- in the redox couple, for dye regeneration.[164–166] The most commonly used counter electrode material is Pt on a conductive ITO or FTO substrate, owing to its excellent electrocatalytic activity for I_3^- reduction, high electrical conductivity for efficient electron transport, and high electrochemical stability in the electrolyte system.[167,168] However, Pt has several drawbacks, such as high-cost, scarcity in nature and poor stability due to corrosion from I_3^- in the redox couple, which limit its application, and hence hampers the large-scale commercialization of DSSCs.[165,169,170]

To address these shortcomings, several materials, such as inorganic compounds,[171,172] carbonaceous materials[173,174] and conductive organic polymers,[175,176] have been investigated as potential alternatives to replace or modify the Pt-based cathodes in DSSCs. Among these, carbonaceous materials, particularly, graphene-based materials are more appealing due to their low-cost, abundance, excellent catalytic activity, large specific surface area, high electrical conductivity, flexibility, and high corrosion resistance.[177–180] Nonetheless, the catalytic activity and electrical conductivity of graphene-based materials are still too low to match those of Pt,[169] which results in relatively poor device performance.

Also, since the electrocatalytic activity of graphene-based materials for I_3^- reduction increases with the number of defect sites, e.g., oxygen functional groups in rGO,[181–183] pristine graphene with a high electrical conductivity, i.e., low charge transfer resistance, tends to have less active sites for catalyzing I_3^- reduction.[169,181] Furthermore, unlike chemical reduction, which increases the electrocatalytic active sites by disrupting the sp^2 conjugation of the graphene lattice, and hence decreases its electrical conductivity, heteroatom doping has been proposed to increase the electrocatalytic active sites, with minor changes in the conjugation length, while increasing the surface hydrophilicity and electrical conductivity.[184,185]

In this regard, Pt/rGO counter electrodes have been used to fabricate highly stable DSSCs, which exhibited PCEs of 5.78,[186] 5.55,[187] 4.73 [188] and 6.64%.[178] Typical cross-sectional field-emission scanning electron microscopy (FE-SEM) images of the Pt and Pt/rGO counter electrodes are shown in Fig. 10 (a) and (b), respectively. Interestingly, most of the Pt/rGO-based devices outperformed their pristine Pt and rGO-based counterparts. Therefore, the incorporation of rGO into the conventional Pt counter electrode not only helps to lower the production cost of

Fig. 9 A schematic diagram of the rGO/polymer–based DSSC.[159]

Table 4 Photovoltaic parameters of DSSCs employing graphene-based electrolytes

Electrolyte	V_{oc} (V)	J_{sc} (mA cm^{-2})	FF	PCE (%)	Ref.
poly(IL)/IL/GO)	0.72	8.84	0.76	4.83	154
GO/PMII-DMII	0.74	9.18	0.75	5.09	155
GO-HMA-TMAI/PMII-DMII	0.75	13.11	0.69	6.78	155
GO-HMA-TBAI/PMII-DMII	0.75	16.85	0.66	8.33	155
GO-gelatin	0.75	7.68	0.70	4.02	153
PEO/PVDF-GO	0.80	14.79	0.75	8.78	156
rGO-PEO	0.65	15.46	0.51	5.07	157
rGO-PMMA	0.87	9.83	0.63	5.38	158
rGO-PEO/PVDF-HFP	0.76	8.50	0.71	4.58	159
GNPLs:PEG-PEO/PVDF-HFP	0.64	13.81	0.62	5.45	161
Graphene-PAA/PEG	0.74	17.80	0.69	9.10	162
Acetonitrile/PVAc-graphene	0.64	6.62	0.43	4.57	163
GQDs-IL	0.50	19.57	0.47	4.57	152
GQDs	0.41	16.95	0.32	2.23	152

DSSCs by reducing the quantity of Pt used on the cathode, but also enhances the device performance and stability.

Pt-free DSSCs consisting of rGO nanosheets as counter electrodes have been developed by Sarker et al.[189] and Sahito et al.,[190] with PCEs of 4.04 and 7.80%, respectively. The rGO-based devices outperformed their GO counterparts, and were comparable to the Pt-based control devices, owing to the higher catalytic activity and enhanced electrical conductivity, resulting from the reduction of GO. This demonstrates the suitability of rGO as a low-cost, efficient and more stable alternative counter electrode material in DSSCs.

In another study, Ma et al.[191] developed a novel Pt-free bilayer counter electrode consisting of an under-layer of aligned CNTs, which served as the transition layer for rGO, and the rGO over-layer, which acted as the catalytic layer. However, the rGO/CNT composite was adversely affected by aggregation, which was addressed by surfactant treatment with non-ionic polyethylene glycol octylphenol ether (Triton X-100), cationic cetylpyridinium chloride (CPC) and anionic sodium dodecyl benzene sulfonate (SDBS). Among these, the CPC-functionalized rGO/CNT (CPC-rGO/CNT) film displayed low interface resistance, and high J_{sc} and FF, which resulted in devices with the best PCE of 3.90%, in comparison with 3.14% for the rGO/CNT-based devices.

Simple and cost-effective polymer/graphene nanocomposites, such as polyaniline (PANI)/graphene,[192–194] PANI/rGO,[195,196] PANI/GO,[197] and poly(3,4-ethylenedioxythiophene):poly(styrenesulfonate) (PEDOT:PSS)/rGO,[198] have also been employed as counter electrodes in DSSCs, which displayed excellent stability and PCEs of 3.59, 7.45, 7.45, 3.98, 5.47, 6.12 and 9.57%, respectively. This was comparable

to the Pt-based devices, and was attributed to a decrease in interfacial charge transfer resistance, owing to the synergy between the high electron-conducting ability of the graphene-based materials and excellent electrocatalytic activity of the conducting polymers. Hence, this paves the way for the future development of conductive polymer/graphene composites, as low-cost, stable and efficient alternatives, well-suited to replace the commonly used Pt counter electrodes in DSSCs.

Recently, N-rGO,[199] aniline (AN)-rGO, and nitrobenzene (NB)-rGO[200] counter electrodes have also been used to fabricate DSSCs, which exhibited PCEs of 4.26, 6.10 and 7.11%, respectively, which were comparable to the Pt control devices, and outperformed the undoped rGO-based DSSCs, demonstrating the significance of doping in enhancing the device performance. Wei et al.[201] also prepared cerium dioxide (CeO$_2$)/N-rGO nanocomposites, and applied them as counter electrodes in DSSCs, which exhibited a PCE of 3.20%, as compared to 2.45 and 1.37% for CeO$_2$/rGO and rGO-based devices, respectively. This was ascribed to the better electrocatalytic activity of the CeO$_2$/N-rGO composite, than rGO and CeO$_2$/rGO, due to the synergistic effect of N and CeO$_2$ on rGO.

Tsai et al. employed nanocomposites of rGO/macrocyclic iron (Fe),[4] rGO/macrocyclic manganese (Mn),[202] rGO/macrocyclic cobalt (Co),[203] and rGO/macrocyclic ytterbium (Yb),[166] as counter electrodes in DSSCs, as illustrated in Fig. 11, which had PCEs of 6.75, 7.47, 7.48 and 7.90%, respectively. The macrocyclic Fe, Mn, Co and Yb complexes were uniformly grafted onto the rGO surface as molecular catalysts. Furthermore, the redox capacity of the macrocyclic complexes, coupled with the large surface area and high electrical conductivity of rGO, led to high electrical conductivity and excellent electrocatalytic activity of the hybrid counter electrodes, resulting in comparable device performance, relative to their Pt-based counterparts. The excellent performance, along with the low cost and easy fabrication of the rGO/macrocyclic complex hybrid materials, shows the potential of the nanocomposites as replacements for the expensive Pt counter electrodes in DSSCs. However, the excessive incorporation of macrocyclic complexes onto rGO often leads to an uneven distribution and aggregation of the complexes, which in turn lowers the electrocatalytic

Fig. 10 Cross-sectional FE–SEM micrographs of (a) Pt and (b) Pt/rGO counter electrodes.[186]

activity of the resulting nanocomposites, and eventually reduces the device performance.

Recently, nanohybrids of cobalt sulfide (Co_3S_4)/rGO,[204] sulfur-doped tricobalt tetraoxide $(S-Co_3O_4)$/rGO,[205] nickel sulfide (NiS)/rGO,[206] cobalt nickel sulfide $(CoNi_2S_4)$/rGO,[207] bismuth sulfide (Bi_2S_3)/rGO,[208] and graphene-based $Cu_2ZnNiSe_4$ with tungsten trioxide (WO_3) nanorods (G-CZNS@W),[209] have been employed as Pt-free counter electrodes in DSSCs. This resulted in devices with impressive PCEs of 8.08, 8.24, 9.50, 9.22, 4.78% and 12.16%, respectively, which were comparable to the Pt control devices. This was attributed to the synergistic effect between the highly catalytic Co_3S_4, $S-Co_3O_4$, NiS, $CoNi_2S_4$, Bi_2S_3 and CZNS@W nanoparticles, and the electrically conductive and electrochemically stable rGO sheets, which paves the way for the development of more efficient Pt-free and low-cost rGO-based nanohybrid counter electrodes, for the future generation of DSSCs.

The photovoltaic parameters of DSSCs employing graphene-based counter electrodes (discussed in this review) are summarized in Table 5. Among these, devices with G-CZNS@W counter electrodes exhibited the best PCE of 12.16%,[209] which outperformed the Pt-based reference devices. This demonstrates that the synergy between graphene-based materials and other Pt-free counter electrode materials, such as CNTs, inorganic compounds and conductive polymers, has the potential to enhance the electrical conductivity, electrocatalytic activity and electrochemical stability, vital for producing low-cost, high performance and sustainable DSSCs.

7. Outlook and perspectives

Among the reported studies, devices with hybrid graphene-based photoanode materials, incorporating transparent electrodes, such as rGO/FTO and GLC/FTO; semiconducting layers, such as graphene/NiS$_2$ and rGO/graphene/TiO$_2$; ruthenium-based

photosensitizers, such as GQDs/N719 and graphene/azulenocyanine/N719, and natural photosensitizers, such as Gracilaria/GQDs and Ulva/GQDs, exhibited superior performance to their corresponding devices based on traditional photoanode materials. Therefore, as a future research direction, it would be crucial to introduce graphene-based nanocomposites into the DSSC photoanode to harness the merits of graphene-based materials, including large-specific surface area, wide and intense absorption spectrum in the visible region, and high electrical conductivity, for more sensitizer loading, enhanced photon absorption, effective photogeneration of electrons and efficient electron transport. In addition, the excellent stability and less environmental impact of graphene-based materials, coupled with the low-cost and environmentally friendly nature of natural dyes, can facilitate the future realization of sustainable and greener photoanode materials. Furthermore, the future integration of graphene-based materials with ruthenium-based dyes can help in reducing the quantity of the toxic, scarce and expensive ruthenium-based dyes required during photosensitizer preparation, thereby facilitating the fabrication of less expensive, clean and safe devices.

On the other hand, devices with the graphene-based quasi-solid state electrolytes, such as PEO/PVDF-GO and graphene-PAA/PEG, exhibited the best PCE and stability, relative to the traditional electrolytes. Thus, future research on graphene-

Fig. 11 A schematic diagram of a DSSC with rGO-based nanocomposite counter electrodes.

Table 5 Photovoltaic parameters of DSSCs with graphene-based counter electrodes

Counter electrode	V_{oc} (V)	J_{sc} (mA cm^{-2})	FF	PCE (%)	Ref.
Pt/rGO	0.69	13.30	0.63	5.78	186
Pt/rGO	0.68	12.27	0.66	5.55	187
Pt/rGO	0.73	7.03	0.69	4.73	188
Pt/rGO	0.73	13.49	0.68	6.64	178
rGO	0.69	9.89	0.59	4.04	189
rGO	0.69	14.35	0.78	7.80	190
rGO/CNT-CPC	0.71	8.80	0.63	3.90	191
rGO/CNT	0.71	7.35	0.60	3.24	191
PANI/graphene	0.71	10.68	0.47	3.59	192
PANI/graphene	0.79	15.50	0.62	7.45	193
PANI/graphene	0.79	15.50	0.62	7.45	194
PANI/rGO	0.63	12.58	0.55	3.98	195
PANI/rGO	0.79	11.50	0.59	5.47	196
PANI/GO	0.71	12.91	0.67	6.12	197
PEDOT:PSS/rGO	0.78	16.11	0.76	9.57	198
N-rGO	0.65	12.06	0.54	4.26	199
AN-rGO	0.72	14.11	0.60	6.10	200
NB-rGO	0.72	15.92	0.62	7.11	200
CeO$_2$/N-rGO	0.65	7.78	0.64	3.20	201
rGO/Fe	0.74	17.69	0.51	6.75	4
rGO/Mn	0.74	17.20	0.58	7.47	202
rGO/Co	0.76	17.34	0.57	7.48	203
rGO/Yb	0.75	15.87	0.66	7.90	166
Co$_3$S$_4$/rGO	0.76	15.70	0.68	8.08	204
S–Co$_3$O$_4$/rGO	0.76	15.90	0.69	8.24	205
S-rGO	0.74	13.00	0.56	5.37	205
NiS/rGO	0.75	16.35	0.78	9.50	206
CoNi$_2$S$_4$/rGO	0.67	16.34	0.84	9.22	207
Bi$_2$S$_3$/rGO	0.72	14.14	0.48	4.78	208
G-CZNS@W	0.88	24.70	0.56	12.16	209
G-CZNS	0.86	21.21	0.48	8.75	209

based composite electrolytes is expected to further improve not only the PCE, but also the long-term operational stability of DSSCs, through the creation of interconnected networks, which not only act as efficient electron transport pathways, but also facilitate the formation of quasi-solid state electrolytes. This, in turn, helps to overcome the leakage and evaporation problems of organic solvents and IL electrolytes, as well as increasing the ionic conductivity of polymer electrolytes.

Also, DSSCs with graphene-based counter electrodes, such as G-CZNS@W, G-CZNS, PEDOT:PSS/rGO and NiS/rGO, outperformed the reference devices based on traditional materials, *e.g.*, Pt. Hence, as a future research direction, it would be vital to take advantage of the synergy between graphene-based materials and other Pt-free counter electrode materials, such as inorganic compounds, CNTs and conductive polymers, to fabricate hybrid graphene-based counter electrodes with improved electrocatalytic activity, electrical conductivity and electrochemical stability. If done, this is envisaged to result in future devices with low-cost, high efficiency and excellent stability.

8. Conclusion

In this review, the recent applications of graphene-based materials in the fabrication of the basic components of DSSCs, such as the photoanodes, electrolytes and counter electrodes, have been presented with a major focus on improving the device performance and sustainability. Hence, this study addresses the current global issues, such as the exhaustion of conventional non-renewable energy sources, environmental pollution, and climate change. Solar energy, a renewable energy source, has been proposed as a potential alternative to the commonly used non-renewable fossil fuels due to its abundance in nature and environmental friendliness. However, the large-scale production of devices utilising solar energy is still limited by the complicated fabrication procedures, high cost and rigidity of the widely used silicon-based solar cells that have already been commercialized. Being motivated by this, several researchers have gained significant research interest in the fabrication of DSSCs, as low-cost, lightweight, flexible and easily scalable alternative devices, with facile fabrication procedures that incorporate readily available materials with less impact on the environment. Nonetheless, the PCE and long-term operational stability of DSSCs are still not favourable for commercial applications. To the best of our knowledge, this can be enhanced by optimizing the properties of the various device components. In this regard, recent efforts have been made to develop new materials for the fabrication of the various DSSC components, of which graphene and its derivatives, such as GO and rGO, are more appealing owing to their remarkable mechanical, chemical, thermal and optoelectronic properties, together with their low-cost, solution-processability, non-toxicity, elemental abundance and flexibility. In particular, the high optical transmittance and high electrical conductivity of graphene-based materials allow their application as photoanodes in DSSCs. On the other hand, their excellent catalytic activity and unique 2D packed structure enable their use as counter electrodes, and renders them with

long-term stability. Also, their large specific surface area, wide and intense absorption spectrum, and continuous interpenetrating networks, facilitate more dye-loading, effective photon harvesting, and efficient charge carrier generation and transport. Although graphene-based DSSCs have attracted considerable research attention, most fabricated devices are still relatively less stable and inefficient for practical applications. Over the last three years, *i.e.*, 2018–2020, the PCE of graphene-based DSSCs has significantly increased from ~0.13 to above 12.00% and can be further improved to approach above 26%, which has been achieved by silicon-based solar cells that have already been commercialized. Among the studies reported in this work, devices with hybrid graphene-based materials, such as rGO/FTO transparent electrodes, graphene/NiS$_2$ semiconducting layers, GQDs/N719 photosensitizers or Gracilaria/GQDs photosensitizers, graphene-PAA/PEG quasi-solid state electrolytes and G-CZNS@W counter electrodes, exhibited superior performance to their corresponding devices based on traditional materials. Therefore, as a future research direction, optimization of the optoelectronic properties of the DSSC components, *via* approaches, such as incorporating novel graphene-based nanocomposites, chemical doping and interfacial engineering, while at the same time reducing the dependency on expensive, scarce and toxic traditional materials, is envisaged to pave the way for the low-cost fabrication, and commercialization of high performance, while ensuring a sustainable future generation, of all-carbon-based DSSCs.

Conflicts of interest

The authors have no conflicts of interest to declare.

Acknowledgements

References

1 W. E. Ghann, H. Kang, J. Uddin, F. A. Chowdhury, S. I. Khondaker, M. Moniruzzaman, M. H. Kabir and M. M. Rahman, *ChemEngineering*, 2019, **3**, 7–19.

2 T. Zahra, K. S. Ahmad, A. G. Thomas, C. Zequine, M. A. Malik and R. K. Gupta, *RSC Adv.*, 2020, **10**, 9854–9867.

3 F. E. Subhan, A. D. Khan, A. D. Khan, N. Ullah, M. Imran and M. Noman, *RSC Adv.*, 2020, **10**, 26631–26638.

4 C.-H. Tsai, W.-C. Huang, W.-S. Wang, C.-J. Shih, W.-F. Chi, Y.-C. Hu and Y.-H. Yu, *J. Colloid Interface Sci.*, 2017, **495**, 111–121.

5 A. Omar, M. S. Ali and N. A. Rahim, *Sol. Energy*, 2020, **207**, 1088–1121.

6 B. W. H. Saes, M. M. Wienk and R. A. J. Janssen, *RSC Adv.*, 2020, **10**, 30176–30185.

7 X. Ke, L. Meng, X. Wan, Y. Cai, H.-H. Gao, Y.-Q.-Q. Yi, Z. Guo, H. Zhang, C. Li and Y. Chen, *Nano Energy*, 2020, **75**, 104988–104995.

8 A. Monreal-Bernal, J. J. Vilatela and R. D. Costa, *Carbon*, 2019, **141**, 488–496.

9 F. Jahantigh, S. M. B. Ghorashi and A. Bayat, *Dyes Pigm.*, 2020, **175**, 108118.

10 S. Suragtkhuu, O. Tserendavag, U. Vandandoo, A. S. R. Bati, M. Bat-Erdene, J. G. Shapter, M. Batmunkh and S. Davaasambuu, *RSC Adv.*, 2020, **10**, 9133–9139.

11 A. Babaei, C. Dreessen, M. Sessolo and H. J. Bolink, *RSC Adv.*, 2020, **10**, 6640–6646.

12 J. F. Lei, S. L. Liu, K. Du, S. J. Lv, C. J. Liu and L. Z. Zhao, *Electrochim. Acta*, 2015, **171**, 66–71.

13 S. P. Lim, A. Pandikumar, N. M. Huang and H. N. Lim, *Int. J. Energy Res.*, 2015, **39**, 812–824.

14 S. Daulay, A. F. Madsuha, E. S. Rosa and A. H. Yuwono, *J. Phys.: Conf. Ser.*, 2019, **1402**, 055101.

15 S. Zhang, J. Jin, D. Li, Z. Fu, S. Gao, S. Cheng, X. Yu and Y. Xiong, *RSC Adv.*, 2019, **9**, 22092–22100.

16 Y. Wu, J. Zhu and L. Huang, *Carbon*, 2019, **143**, 610–640.

17 E. T. Mombeshora, P. G. Ndungu, A. L. L. Jarvis and V. O. Nyamori, *Mater. Chem. Phys.*, 2018, **213**, 102–112.

18 B. Tang, H. Yu, H. Peng, Z. Wang, S. Li, T. Ma and W. Huang, *RSC Adv.*, 2018, **8**, 29220–29227.

19 M. Ahmad and S. R. P. Silva, *Carbon*, 2019, **158**, 24–44.

20 D. G. Papageorgiou, I. A. Kinloch and R. J. Young, *Prog. Mater. Sci.*, 2017, **90**, 75–127.

21 T. Mahmoudi, W. Y. Rho, H. Y. Yang, S. R. Silva and Y. B. Hahn, *Chem. Commun.*, 2014, **50**, 8705–8708.

22 W. Meng, X. Zhou, Z. Qiu, C. Liu, J. Chen, W. Yue, M. Wang and H. Bi, *Carbon*, 2016, **96**, 532–540.

23 S. Stankovich, D. A. Dikin, R. D. Piner, K. A. Kohlhaas, A. Kleinhammes, Y. Jia, Y. Wu, S. B. T. Nguyen and R. S. Ruoff, *Carbon*, 2007, **45**, 1558–1565.

24 J. Zhang, L. Lin, K. Jia, L. Sun, H. Peng and Z. Liu, *Adv. Mater.*, 2020, **32**, 1903266–1903292.

25 E. S. Agudosi, E. C. Abdullah, A. Numan, N. M. Mubarak, M. Khalid and N. Omar, *Crit. Rev. Solid State Mater. Sci.*, 2020, **45**, 339–377.

26 W. Norimatsu, K. Matsuda, T. Terasawa, N. Takata, A. Masumori, K. Ito, K. Oda, T. Ito, A. Endo, R. Funahashi and M. Kusunoki, *Nanotechnology*, 2020, **31**, 145711.

27 K. R. Nandanapalli, D. Mudusu and S. Lee, *Carbon*, 2019, **152**, 954–985.

28 W. Yu, L. Sisi, Y. Haiyan and L. Jie, *RSC Adv.*, 2020, **10**, 15328–15345.

29 S. Pei and H.-M. Cheng, *Carbon*, 2012, **50**, 3210–3228.

30 T. Mahmoodi and Y.-B. Hahn, *Nano Energy*, 2018, **47**, 51–65.

31 G. Eda, Y.-Y. Lin, S. Miller, C.-W. Chen, W.-F. Su and M. Chhowalla, *Appl. Phys. Lett.*, 2008, **92**, 233305.

32 T. Majumder and S. P. Mondal, *Bull. Mater. Sci.*, 2019, **42**, 65–69.

33 D. Krishnamoorthy and A. Prakasam, *Inorg. Chem. Commun.*, 2020, **119**, 108063.

34 K. Yoshikawa, H. Kawasaki, W. Yoshida, T. Irie, K. Konishi, K. Nakano, T. Uto, D. Adachi, M. Kanematsu, H. Uzu and K. Yamamoto, *Nat. Energy*, 2017, **2**, 17032–17039.

35 A. Saedi, A. M. Moradi, S. Kimiagar and H. A. Panahi, *Int. J. Environ. Res.*, 2020, **14**, 393–402.

36 D. K. Kumar, J. Kříž, N. Bennett, B. Chen, H. Upadhayaya, K. R. Reddy and V. Sadhu, *Mater. Sci. Energy Technol.*, 2020, **3**, 472–481.

37 N. Chander and V. K. Komarala, *Indian J. Pure Appl. Phys.*, 2017, **55**, 737–744.

38 M. Z. Iqbal and A.-U. Rehman, *Sol. Energy*, 2018, **169**, 634–647.

39 K. Sharma, C. Sharma and S. S. Sharma, *Nanoscale Res. Lett.*, 2018, **13**, 381.

40 A. Abdukarimov, S. Shah, L. P. Teo, M. H. Buraidah, Z. H. Z. Abidin, O. O. Mamatkarimov and A. K. Arof, *Opt. Quantum Electron.*, 2020, **52**, 152–166.

41 M. Hosseinnezhad, K. Gharanjig, M. K. Yazdi, P. Zarrintaj, S. Moradian, M. R. Saeb and F. J. Stadler, *J. Alloys Compd.*, 2020, **828**, 154329–154344.

42 A. Iwan and A. Chuchmała, *Prog. Polym. Sci.*, 2012, **37**, 1805–1828.

43 E. Muchuweni, T. S. Sathiaraj and H. Nyakotyo, *Appl. Surf. Sci.*, 2016, **390**, 570–577.

44 E. Muchuweni, T. S. Sathiaraj and H. Nyakotyo, *Ceram. Int.*, 2016, **42**, 10066–10070.

45 E. Muchuweni, T. S. Sathiaraj and H. Nyakotyo, *Heliyon*, 2017, **3**, e00285.

46 E. Muchuweni, T. S. Sathiaraj and H. Nyakotyo, *J. Alloys Compd.*, 2017, **721**, 45–54.

47 A. Andersson, N. Johansson, P. Bröms, N. Yu, D. Lupo and W. R. Salaneck, *Adv. Mater.*, 1998, **10**, 859.

48 P. Varshney, M. Deepa, N. Sharma and S. A. Agnihotry, *Solid State Ionics*, 2002, **152**, 877–881.

49 J. Y. Ho, J. K. Se, J. H. Hwang, Y. S. Shim, S.-G. Jung, Y. W. Park and J. Byeong-Kwon, *Sci. Rep.*, 2016, **6**, 34150.

50 D. P. Langley, G. Giusti, M. Lagrange, R. Collins, C. Jiménez, Y. Bréchet and D. Bellet, *Sol. Energy Mater. Sol. Cells*, 2014, **125**, 318–324.

51 L. S. Priyadharshni and M. Selvaraj, *Int. J. Polym. Mater. Polym. Biomater.*, 2014, **64**, 47–53.

52 J. E. McCarthy, C. A. Hanley, V. G. Lambertini and Y. K. Gun'ko, *Fabrication of highly transparent and conductive PEDOT:PSS thin films for flexible electrode applications*, Nanocon.Eu, Czech Republic; 2013.

53 J. Nomoto, T. Hirano, T. Miyata and T. Minami, *Thin Solid Films*, 2011, **520**, 1400–1406.

54 D. Liu, S. Ren, X. Ma, C. Liu, L. Wu, W. Li, J. Zhang and L. Feng, *RSC Adv.*, 2017, **7**, 8295–8302.

55 A. Du Pasquier, H. E. Unalan, A. Kanwal, S. Miller and M. Chhowalla, *Appl. Phys. Lett.*, 2005, **87**, 203511.

56 X. Yu, R. Rajaman, K. A. Stelson and T. Cui, *J. Nanosci. Nanotechnol.*, 2006, **6**, 1939–1944.

57 M. Song, H.-K. Seo, S. Ameen, M. S. Akhtar and H.-S. Shin, *Electrochim. Acta*, 2014, **115**, 559–565.

58 X. Wang, L. Zhi and K. Müllen, *Nano Lett.*, 2008, **8**, 323–327.

59 P. Dong, Y. Zhu, J. Zhang, C. Peng, Z. Yan, L. Li, Z. Peng, G. Ruan, W. Xiao, H. Lin, J. M. Tour and J. Lou, *J. Phys. Chem. C*, 2014, **118**, 25863–25868.

60 T. Chen, W. Hu, J. Song, G. H. Guai and C. M. Li, *Adv. Funct. Mater.*, 2012, **22**, 5245–5250.

61 M. U. Shahid, N. M. Mohamed, M. Khatani, A. S. Muhsan, A. Samsudin, M. I. Irshad and S. N. A. Zaine, *AIP Conf. Proc.*, 2017, **1901**, 020004.

62 K.-M. Roh, E.-H. Jo, H. Chang, T. H. Han and H. D. Jang, *J. Solid State Chem.*, 2015, **224**, 71–75.

63 G. S. Selopal, R. Milan, L. Ortolani, V. Morandi, R. Rizzoli, G. Sberveglieri, G. P. Veronese, A. Vomiero and I. Concina, *Sol. Energy Mater. Sol. Cells*, 2015, **135**, 99–105.

64 N. A. F. Al-Rawashdeh, B. A. Albiss and M. H. I. Yousef, *IOP Conf. Ser.: Mater. Sci. Eng.*, 2018, **305**, 012019–012032.

65 C. Y. Neo and J. Ouyang, *J. Power Sources*, 2013, **222**, 161–168.

66 M. R. Subramaniam, D. Kumaresan, S. Jothi, J. D. McGettrick and T. M. Watson, *Appl. Surf. Sci.*, 2018, **428**, 439–447.

67 C.-H. Shan, H. Zhang, W.-L. Chen, Z.-M. Su and E.-B. Wang, *J. Mater. Chem. A*, 2016, **4**, 3297–3303.

68 X. B. Chen and S. S. Mao, *Chem. Rev.*, 2007, **107**, 2891–2959.

69 R. Raja, M. Govindaraj, M. D. Antony, K. Krishnan, E. Velusamy, A. Sambandam, M. Subbaiah and V. W. Rayar, *J. Solid State Electrochem.*, 2017, **21**, 891–903.

70 M. Grätzel, *J. Photochem. Photobiol., A*, 2004, **164**, 3–14.

71 A. Fujishima, X. Zhang and D. A. Tryk, *Surf. Sci. Rep.*, 2008, **63**, 515–582.

72 J. Y. Liao, B. X. Lei, D. B. Kuang and C. Y. Su, *Energy Environ. Sci.*, 2011, **4**, 4079–4085.

73 M. Motlak, N. A. M. Barakat, M. S. Akhtar, A. G. El-Deen, M. Obaid, C. S. Kim, K. A. Khalil and A. A. Almajid, *Chem. Eng. J.*, 2015, **268**, 153–161.

74 H. Cai, J. Li, X. Xu, H. Tang, J. Luo, K. Binnemans, J. Fransaer and D. E. De Vos, *J. Alloys Compd.*, 2017, **697**, 132–137.

75 A. K. Chandiran, M. Abdi-Jalebi, M. K. Nazeeruddin and M. Grätzel, *ACS Nano*, 2014, **8**, 2261–2268.

76 J. V. Patil, S. S. Mali, J. S. Shaikh, A. P. Patil, P. S. Patil and C. K. Hong, *Synth. Met.*, 2019, **256**, 116146–116154.

77 S. Bae, H. Kim, Y. Lee, X. Xu, J. Park, Y. Zheng, *et al.*, *Nat. Nanotechnol.*, 2010, **5**, 574–578.

78 S. Bhaviripudi, X. Jia, M. S. Dresselhaus and J. Kong, *Nano Lett.*, 2010, **10**, 4128–4133.

79 Z. Xiang, X. Zhou, G. Wan, G. Zhang and D. Cao, *ACS Sustainable Chem. Eng.*, 2014, **2**, 1234–1240.

80 A. M. Ramli, M. Z. Razali and N. A. Ludin, *Malaysian J. Anal. Sci.*, 2017, **21**, 928–940.

81 S. W. Chong, C. W. Lai, J. C. Juan and B. F. Leo, *Sol. Energy*, 2019, **191**, 663–671.

82 V. S. Manikandan, A. K. Palai, S. Mohanty and S. K. Nayak, *J. Alloys Compd.*, 2019, **793**, 400–409.

83 X. H. Yau, F. W. Low, C. S. Khe, C. W. Lai, S. K. Tiong and N. Amin, *PLoS One*, 2020, **15**, e0228322.

84 Y.-H. Nien, H.-H. Chen, H.-H. Hsu, P.-Y. Kuo, J.-C. Chou, C.-H. Lai, G.-M. Hu, C.-H. Kuo and C.-C. Ko, *Vacuum*, 2019, **167**, 47–53.

85 C. Wang, Y. Zhou, Z. Ge, R. Shi, T. Chen, Z. Chen and J. Liu, *Colloid Interface Sci. Commun.*, 2020, **39**, 100313–100318.

86 K. Surana, S. Konwar, P. K. Singh and B. Bhattacharya, *J. Alloys Compd.*, 2019, **788**, 672–676.

87 F. W. Low, C. W. Lai and S. B. A. Hamid, *J. Mater. Sci.: Mater. Electron.*, 2017, **28**, 3819–3836.

88 L. Wei, P. Wang, Y. Yang, Y. Dong, R. Fan, W. Song, Y. Qiu, Y. Yang and T. Luan, *Thin Solid Films*, 2017, **639**, 12–21.

89 S. A. Kazmi, S. Hameed, A. S. Ahmed, M. Arshad and A. Azam, *J. Alloys Compd.*, 2017, **691**, 659–665.

90 F. W. Low, C. W. Lai and S. B. Abd Hamid, *Ceram. Int.*, 2017, **43**, 625–633.

91 K. A. Kumar, K. Subalakshmi and J. Senthilselvan, *Mater. Sci. Semicond. Process.*, 2019, **96**, 104–115.

92 Y. Zhang, C. Wang, Z. Yuan, L. Zhang and L. Yin, *Eur. J. Inorg. Chem.*, 2017, **2017**, 2281–2288.

93 H. M. A. Javed, A. A. Qureshi, M. S. Mustafa, W. Que, M. S. Mahr, A. Shaheen, J. Iqbal, S. Saleem, M. Jamshaid and A. Mahmood, *Opt. Commun.*, 2019, **453**, 124408–124415.

94 K. Pattarith and Y. Areerob, *Renewable Energy*, 2020, **7**, 1–10.

95 T. T. N. Le, V. C. Le, T. P. Le, T. T. M. Nguyen, H. D. Ho, K. H. Le, M. H. Tran, T. H. Nguyen, T. L. C. Pham, H. M. Nam, M. T. Phong and N. H. Hieu, *Chem. Eng. Trans.*, 2020, **78**, 61–66.

96 C. Jeganathan, T. C. S. Girisun, S. Vijaya and S. Anandan, *Electrochim. Acta*, 2019, **319**, 909–921.

97 S. N. Sadikin, M. Y. A. Rahman, A. A. Umar and T. H. T. Aziz, *Superlattices Microstruct.*, 2019, **128**, 92–98.

98 M. Batmunkh, M. Dadkhah, C. J. Shearer, M. J. Biggs and J. G. Shapter, *Appl. Surf. Sci.*, 2016, **387**, 690–697.

99 K. Basu, G. S. Selopal, M. Mohammadnezad, R. Akilimali, Z. M. Wang, H. Zhao, F. Vetrone and F. Rosei, *Electrochim. Acta*, 2020, **349**, 136409–136417.

100 N. Gao, T. Wan, Z. Xu, L. Ma, S. Ramakrishna and Y. Liu, *Mater. Chem. Phys.*, 2020, **225**, 123542.

101 D. Krishnamoorthy and A. Prakasam, *Inorg. Chem. Commun.*, 2020, **11**, 108016.

102 D. K. Kumar, D. Suazo-Davila, D. García-Torres, N. P. Cook, A. Ivaturi, M.-H. Hsu, A. A. Martí, C. R. Cabrera, B. Chen, N. Bennett and H. M. Upadhyaya, *Electrochim. Acta*, 2019, **305**, 278–284.

103 M. N. Mustafa and Y. Sulaiman, *J. Electroanal. Chem.*, 2020, **876**, 114516.

104 S.-J. Lin, K.-C. Lee, J.-L. Wu and J.-Y. Wu, *Sol. Energy*, 2012, **86**, 2600–2605.

105 A. C. M. S. Esteban and E. P. Enriquez, *Sol. Energy*, 2013, **98**, 392–399.

106 J. Gong, J. Liang and K. Sumathy, *Renewable Sustainable Energy Rev.*, 2012, **16**, 5848–5860.

107 A. Hagfeldt, G. Boschloo, L. Sun, L. Kloo and H. Pettersson, *Chem. Rev.*, 2010, **110**, 6595–6663.

108 Z. Pan, I. Mora-Seró, Q. Shen, H. Zhang, Y. Li, K. Zhao, J. Wang, X. Zhong and J. Bisquert, *J. Am. Chem. Soc.*, 2014, **136**, 9203–9210.

109 S. Anandan, *Sol. Energy Mater. Sol. Cells*, 2007, **91**, 843–846.

110 S. Furukawa, H. Iino, T. Iwamoto, K. Kukita and S. Yamauchi, *Thin Solid Films*, 2009, **518**, 526–529.

111 G. Calogero, J.-H. Yum, A. Sinopoli, G. Di Marco, M. Graetzel and M. K. Nazeeruddin, *Sol. Energy*, 2012, **86**, 1563–1575.

112 C. G. Garcia, A. S. Polo and N. Y. M. Iha, *J. Photochem. Photobiol., A*, 2003, **160**, 87–91.

113 M. R. Narayan, *Renewable Sustainable Energy Rev.*, 2011, **16**, 208–215.

114 J. Chang, J. Yang, P. Ma, D. Wu, L. Tian, Z. Gao, K. Jiang and L. Yang, *J. Colloid Interface Sci.*, 2013, **394**, 231–236.

115 M. Ismail, N. A. Ludin, M. A. Ibrahim, N. H. Hamid, M. S. Zulfakar, N. M. Mohamed and K. Sopian, *AIP Conf. Proc.*, 2017, **1838**, 020017.

116 R. Kaur, K.-H. Kim and A. Deep, *Appl. Surf. Sci.*, 2017, **396**, 1303–1309.

117 A. V. Vinogradov, H. Zaake-Hertling, E. Hey-Hawkins, A. V. Agafonov, G. A. Seisenbaeva, V. G. Kessler and V. V. Vinogradov, *Chem. Commun.*, 2014, **50**, 10210–10213.

118 D. Y. Lee, C. Y. Shin, S. J. Yoon, H. Y. Lee, W. Lee, N. K. Shrestha, J. K. Lee and S.-H. Han, *Sci. Rep.*, 2014, **4**, 3930.

119 T. Gatti, N. Manfredi, C. Boldrini, F. Lamberti, A. Abbotto and E. Menna, *Carbon*, 2017, **115**, 746–753.

120 M. S. Wahab, A. F. Madsuha, E. S. Rosa and A. H. Yuwono, *J. Phys.: Conf. Ser.*, 2019, **1402**, 066017.

121 M. Volland, A. Lennert, A. Roth, M. Ince, T. Torres and D. M. Guldi, *Nanoscale*, 2019, **11**, 10709–10715.

122 F. Huang, J. Hou, Q. Zhang, Y. Wang, R. C. Masse, S. Peng, H. Wang, J. Liu and G. Cao, *Nano Energy*, 2016, **26**, 114–122.

123 J. H. Bang and P. V. Kamat, *ACS Nano*, 2009, **3**, 1467–1476.

124 G.-H. Kim, B. Walker, D. Zhitomirsky, J. Heo, S.-J. Ko, J. Park, E. H. Sargent and J. Y. Kim, *Nano Energy*, 2015, **13**, 491–499.

125 J. Zhang, J. Gao, C. P. Church, E. M. Miller, J. M. Luther, V. I. Klimov and M. C. Beard, *Nano Lett.*, 2014, **14**, 6010–6015.

126 J. Peng, W. Gao, B. K. Gupta, Z. Liu, R. R. Aburto, L. Ge, L. Song, L. B. Alemany, X. Zhan, G. Gao, S. A. Vithayathil, B. A. Kaipparettu, A. A. Marti, T. Hayashi, J. Zhu and P. M. Ajayan, *Nano Lett.*, 2012, **12**, 844–849.

127 G. Zamiri and S. Bagheri, *J. Colloid Interface Sci.*, 2018, **511**, 318–324.

128 F. Jahantigh, S. M. B. Ghorash and S. Mozaffari, *J. Solid State Electrochem.*, 2020, **24**, 883–889.

129 W. Yang, I.-W. Park, J. M. Lee and H. Choi, *J. Nanosci. Nanotechnol.*, 2020, **20**, 3432–3436.

130 A. Sacco, S. Porro, A. Lamberti, M. Gerosa, M. Castellino, A. Chiodoni and S. Bianco, *Electrochim. Acta*, 2014, **131**, 154–159.

131 J. Wu, Z. Lan, J. Lin, M. Huang, Y. Huang, L. Fan and G. Luo, *Chem. Rev.*, 2015, **115**, 2136–2173.

132 J. Wu, Z. Lan, J. Lin, M. Huang and P. Li, *J. Power Sources*, 2007, **173**, 585–591.

133 D. Wei, *Int. J. Mol. Sci.*, 2010, **11**, 1103–1113.

134 I. Ahmad, U. Khan and Y. K. Gun'ko, *J. Mater. Chem.*, 2011, **21**, 16990–16996.

135 K. Xu, *Chem. Rev.*, 2004, **104**, 4303–4418.

136 J. H. Wu, Z. Lan, J. M. Lin, M. L. Huang, S. C. Hao, T. Sato and S. Yin, *Adv. Mater.*, 2007, **19**, 4006–4011.

137 F. Gray, J. MacCallum, C. Vincent and J. Giles, *Macromolecules*, 1988, **21**, 392–397.

138 S. Mathew, A. Yella, P. Gao, R. H. Baker, B. F. E. Curchod, N. A. Astani, I. Tavernelli, U. Rothlisberger, M. K. Nazeeruddin and M. Grätzel, *Nat. Chem.*, 2014, **6**, 242–247.

139 A. Sepehrifard, B. A. Kamino, T. P. Bender and S. Morin, *ACS Appl. Mater. Interfaces*, 2012, **4**, 6211–6215.

140 C. S. Karthikeyan, H. Wietasch and M. Thelakkat, *Adv. Mater.*, 2007, **19**, 1091–1095.

141 G. Kumara, A. Konno, K. Shiratsuchi, J. Tsukahara and K. Tennakone, *Chem. Mater.*, 2002, **14**, 954–955.

142 K. Tennakone, G. Senadeera, D. De Silva and I. Kottegoda, *Appl. Phys. Lett.*, 2000, **77**, 2367–2369.

143 M. Singh, V. K. Singh, K. Surana, B. Bhattacharya, P. K. Singh and H.-W. Rhee, *J. Ind. Eng. Chem.*, 2013, **19**, 819–822.

144 M. Hu, J. Sun, Y. Rong, Y. Yang, L. Liu, X. Li, M. Forsyth, D. R. MacFarlane and H. Han, *J. Power Sources*, 2014, **248**, 283–288.

145 J. H. Wu, S. C. Hao, Z. Lan, J. M. Lin, M. L. Huang, Y. F. Huang, L. Q. Fang, S. Yin and T. Sato, *Adv. Funct. Mater.*, 2007, **17**, 2645–2652.

146 Y. Liu, J. Y. Lee and L. Hong, *J. Power Sources*, 2004, **129**, 303–311.

147 M. Biancardo, K. West and F. C. Krebs, *Sol. Energy Mater. Sol. Cells*, 2006, **90**, 2575–2588.

148 W. Kubo, T. Kitamura, K. Hanabusa, Y. Wada and S. Yanagida, *Chem. Commun.*, 2002, **2002**, 374–375.

149 M. S. Akhtar, S. Kwon, F. J. Stadler and O. B. Yang, *Nanoscale*, 2013, **5**, 5403–5411.

150 M. Galiński, A. Lewandowski and I. Stępniak, *Electrochim. Acta*, 2006, **51**, 5567–5580.

151 R. D. Rogers and K. R. Seddon, *Science*, 2003, **302**, 792–793.

152 A. Porfarzollah, R. Mohammad-Rezaei and M. Bagheri, *J. Mater. Sci.: Mater. Electron.*, 2020, **31**, 2288–2297.

153 M. Khannam, R. Boruah and S. K. Dolui, *J. Photochem. Photobiol., A*, 2017, **335**, 248–258.

154 B. Lin, T. Feng, F. Chu, S. Zhang, N. Yuan and J. Ding, *RSC Adv.*, 2015, **5**, 57216–57222.

155 E. Kowsari and M. R. Chirani, *Carbon*, 2017, **118**, 384–392.

156 S. Venkatesan, E. S. Darlim, M.-H. Tsai, H. Teng and Y.-L. Lee, *ACS Appl. Mater. Interfaces*, 2018, **10**, 10955–10964.

157 P. E. Marchezi, G. G. Sonai, M. K. Hirata, M. A. Schiavon and A. F. Nogueira, *J. Phys. Chem. C*, 2016, **120**, 23368–23376.

158 R. R. Shrivatsav, V. Mahalingam, E. R. L. Narayanan, N. N. Balaji, M. Balu, R. K. Prasad and D. Kumaresan, *Mater. Res. Express*, 2018, **5**, 046204.

159 K. Prabakaran, P. J. Jandas, S. Mohanty and S. K. Nayak, *Sol. Energy*, 2018, **170**, 442–453.

160 S. Kumar, V. S. Manilandan, S. K. Panda, S. P. Senanayak and A. K. Palai, *Sol. Energy*, 2020, **208**, 949–956.

161 P. Manafi, H. Nazockdast, M. Karimi, M. Sadighi and L. Magagnin, *Polymers*, 2020, **12**, 1443–1465.

162 J. Zheng, *J. Power Sources*, 2017, **348**, 239–245.

163 S. Rehman, M. Noman, A. D. Khan, A. Saboor, M. S. Ahmad and H. U. Khan, *Optik*, 2020, **202**, 163591.

164 J. Halme, P. Vahermaa, K. Miettunen and P. Lund, *Adv. Mater.*, 2010, **22**, E210–E234.

165 M.-H. Yeh, L.-Y. Lin, J.-S. Su, Y.-A. Leu, R. Vittal, C.-L. Sun and K.-C. Ho, *ChemElectroChem*, 2014, **1**, 416–425.

166 C.-H. Tsai, S.-L. Shiu, W.-C. Lin, Y.-R. Chou and Y.-H. Yu, *Org. Electron.*, 2019, **64**, 166–175.

167 N. Papageorgiou, W. F. Maierand and M. Grätzel, *J. Electrochem. Soc.*, 1997, **144**, 876–884.

168 G. Calogero, P. Calandra, A. Irrera, A. Sinopoli, I. Citro and G. Di Marco, *Energy Environ. Sci.*, 2011, **4**, 1838–1844.

169 Y. Xue, J. Liu, H. Chen, R. Wang, D. Li, J. Qu and L. Dai, *Angew. Chem., Int. Ed.*, 2012, **51**, 12124–12127.

170 W. Yang, X. Xu, Z. Li, F. Yang, L. Zhang, Y. Li, A. Wang and S. Chen, *Carbon*, 2016, **96**, 947–954.

171 M. Wu, X. Lin, Y. Wang, L. Wang, W. Guo, D. Qi, X. Peng, A. Hagfeldt, M. Grätzel and T. Ma, *J. Am. Chem. Soc.*, 2012, **134**, 3419–3428.

172 X. Xin, M. He, W. Han, J. Jung and Z. Lin, *Angew. Chem., Int. Ed.*, 2011, **50**, 11739–11742.

173 Z. Li, F. Gong, G. Zhou and Z. S. Wang, *J. Phys. Chem. C*, 2013, **117**, 6561–6566.

174 L. Kavan, J. H. Yum and M. Grätzel, *ACS Nano*, 2011, **5**, 165–172.

175 J. G. Chen, H. Y. Wei and K. C. Ho, *Sol. Energy Mater. Sol. Cells*, 2007, **91**, 1472–1477.

176 J. Wu, Q. Li, L. Fan, Z. Lan, P. Li, J. Lin and S. Hao, *J. Power Sources*, 2008, **181**, 172–176.

177 M.-Y. Yen, C.-C. Teng, M.-C. Hsiao, P.-I. Liu, W.-P. Chuang, C.-C. M. Ma, C.-K. Hsieh, M.-C. Tsai and C.-H. Tsai, *J. Mater. Chem.*, 2011, **21**, 12880–12888.

178 L. V. Cuong, N. D. Thinh, L. T. Nghia, N. D. Khoa, L. K. Hung, H. H. Dat, P. T. Khang, N. T. Hoang, P. T. L. Chau, M. T. Phong and N. H. Hieu, *Inorg. Chem. Commun.*, 2020, **118**, 108033–108038.

179 Z. Teng, H. Lv, C. Wang, H. Xue, H. Pang and G. Wang, *Carbon*, 2011, **113**, 63–75.

180 T. Chiang, C. Chou, D. Wu and C. Hsiung, *Adv. Mater. Res.*, 2011, **239**, 1747–1750.

181 D. J. B. Joseph, D. Roy-Mayhew, C. Punckt and I. A. Aksay, *ACS Nano*, 2010, **4**, 6203–6211.

182 M. Yu, J. Zhang, S. Li, Y. Meng and J. Liu, *J. Power Sources*, 2016, **308**, 44–51.

183 H. Zheng, C. Y. Neo, X. Mei, J. Qiu and J. Ouyang, *J. Mater. Chem.*, 2012, **22**, 1446.

184 D. S. Yu, E. Nagelli, F. Du and L. M. Dai, *J. Phys. Chem. Lett.*, 2010, **1**, 2165–2173.

185 S. B. Yang, X. L. Feng, X. C. Wang and K. Müllen, *Angew. Chem.*, 2011, **123**, 5451–5455; *Angew. Chem., Int. Ed.*, 2011, **50**, 5339–5343.

186 N. T. Khoa, D. V. Thuan, S. W. Kim, S. Park, T. V. Tam, W. M. Choi, S. Cao, E. J. Kim and S. H. Hahn, *RSC Adv.*, 2016, **6**, 1535–1541.

187 M. Yu, X. Wu, J. Zhang, Y. Meng, Y. Ma, J. Liu and S. Li, *Electrochim. Acta*, 2017, **258**, 485–494.

188 N. D. Thinh, V. O. Le, L. T. T. Nghia, L. V. Cuong, N. T. T. My, N. T. K. Tuyet, N. T. Hoang and N. H. Hieu, *Vietnam J. Chem.*, 2019, **57**, 411–417.

189 S. Sarker, K.-S. Lee, H. W. Seo, Y.-K. Jin and D. M. Kim, *Sol. Energy*, 2017, **158**(2017), 42–48.

190 I. A. Sahito, K. C. Sun, A. A. Arbab and S. H. Jeong, *Sol. Energy*, 2019, **190**, 112–118.

191 J. Ma, H.-L. Yang and W.-H. Ren, *J. Nanosci. Nanotechnol.*, 2020, **20**, 1749–1755.

192 M. U. Shahid, N. M. Mohamed, A. S. Muhsan, R. Bashiri, A. E. Shamsudin and S. N. A. Zaine, *Diamond Relat. Mater.*, 2019, **94**, 242–251.

193 U. Mehmood, N. A. Karim, H. F. Zahid, T. Asif and M. Younas, *Mater. Lett.*, 2019, **256**, 126651–126653.

194 U. Mehmood, H. Asghar, F. Babar and M. Younas, *Sol. Energy*, 2020, **196**, 132–136.

195 H. Seema, Z. Zafar and A. Samreen, *Arabian J. Chem.*, 2020, **13**, 4978–4986.

196 K. Mohan, A. Bora, R. S. Roy, B. C. Nath and S. K. Dolui, *Sol. Energy*, 2019, **186**, 360–369.

197 H. G. Lemos, D. Barba, G. S. Selopal, C. Wang, Z. M. Wang, A. Duong, F. Rosei, S. F. Santos and E. C. Venancio, *Sol. Energy*, 2020, **207**, 1202–1213.

198 V. Sudhakar, A. K. Singh and M. K. Chini, *ACS Appl. Electron. Mater.*, 2020, **2**, 626–634.

199 L. Wei, P. Wang, Y. Yang, R. Luo, J. Li, X. Gu, Z. Zhan, Y. Dong, W. Song and R. Fan, *J. Nanopart. Res.*, 2018, **20**, 110–121.

200 J. Rakspun, Y.-J. Chiang, J.-Y. Chen, C.-Y. Yeh, V. Amornkitbamrung, N. Chanlek, V. Vailikhit and P. Hasin, *Sol. Energy Mater.*, 2020, **203**, 175–186.

201 L. Wei, Q. Wu, Y. Yang, B. Jiang, G. Sun, J. Feng, F. Yu, Y. Kang and G. Dong, *J. Mater. Res.*, 2020, **35**, 1–11.

202 C.-H. Tsai, C.-J. Shih, Y.-R. Chou, W.-F. Chi, W.-C. Huang and Y.-H. Yu, *Org. Electron.*, 2018, **52**, 51–60.

203 C.-H. Tsai, C.-J. Shih, W.-S. Wang, W.-F. Chi, W.-C. Huang, Y.-C. Hu and Y.-H. Yu, *Appl. Surf. Sci.*, 2018, **434**, 412–422.

204 T. Jiang, S. Yang, P. Dai, X. Yu, Z. Bai, M. Wu, G. Li and C. Tu, *Electrochim. Acta*, 2018, **261**, 143–150.

205 T. Jiang, N. Yin, Z. Bai, P. Dai, X. Yu, M. Wu and G. Li, *Appl. Surf. Sci.*, 2018, **450**, 219–227.

206 A. Sarkar, A. K. Chakraborty and S. Bera, *Sol. Energy Mater. Sol. Cells*, 2018, **182**, 314–320.

207 A. Sarkar, S. Bera and A. K. Chakraborty, *Sol. Energy*, 2020, **208**, 139–149.

208 I. Y. Bu, *Optik*, 2020, **217**, 164868–164873.

209 W. C. Oh, K. Y. Cho, C. H. Jung and Y. Areerob, *Sci. Rep.*, 2020, **10**, 4738–4747.